THESIS FOR THE DEGREE OF DOCTOR OF PHILOSOPHY

Microcombs for ultrafast optical interferometry

Israel Rebolledo-Salgado

CHALMERS

Photonics Laboratory
Department of Microtechnology and Nanoscience (MC2)
Chalmers University of Technology
Göteborg, Sweden, 2023

Microcombs for ultrafast optical interferometry
Israel Rebolledo Salgado

ISBN 978-91-7905-958-3
Doktorsavhandlingar vid Chalmers tekniska högskola
Ny serie nr 5424
ISSN 0346-718X

Photonics Laboratory
Department of Microtechnology and Nanoscience (MC2)
Chalmers University of Technology
SE–412 96 Göteborg
Sweden
Telephone: +46 (0)31–772 10 00

Front cover illustration: The schematic of two frequency combs generated in photonic molecules performing dual-comb spectroscopy. One of the combs interacts with a sample and the second comb is used to recover the information encoded.

Printed in Sweden by
Reproservice
Chalmers Tekniska Högskola
Göteborg, Sweden, 2023

Microcombs for ultrafast optical interferometry
Israel Rebolledo-Salgado
Photonics Laboratory
Department of Microtechnology and Nanoscience (MC2)
Chalmers University of Technology

Abstract

The optical frequency comb has revolutionized the field of laser spectroscopy. This type of laser, characterized by an array of uniformly spaced and coherent laser lines, finds promise in photonic platforms for the integration of chip-scale spectrometers. On-chip frequency comb generation can be achieved through microresonators, driven by a single-frequency laser, yielding ultrashort light pulses with a broad spectral bandwidth.

In this thesis, linear interferometry techniques using frequency combs are analyzed, particularly the dual-comb configuration. By using two-frequency combs, this technique enables the optical sampling of a device under test with high resolution and short measurement times. The interest for implementing this technique using microcombs has attracted a high interest, however, its realization is still challenging.

This work studies the dynamics of microcomb generation and their impact on its spectral properties. As a result, it is proposed different methods to stabilize their output which has allowed us to implement dual-comb interferometry for the first time using platicon microcombs. Additionally, a method to tune a microcomb is proposed, potentially overcoming the limitation imposed by sparse spectral sampling, primarily determined by the comb spacing.

Furthermore, the dynamics of spectral broadening are investigated, resulting in the generation of coherent octave-spanning spectra using ultra-low loss nano-photonic waveguides. Overall, the results of this thesis underline the capacity of chip-scale frequency combs to offer extensive spectral coverage, high resolution, sensitivity, and rapid measurement times in optical interferometry.

Keywords: optical frequency combs, microcombs, pulses, nonlinear optics, interferometry, integrated photonics, supercontinuum generation

Sammanfattning

Den optiska frekvenskammen har revolutionerat forskningsområdet laserspektroskopi. Denna typ av laser, som kännetecknas av en rad likformigt fördelade och koherenta laserlinjer, har visat sig vara särskillt lovande för chipintegrerad spektrometeri. Frekvenskamgenerering på chip kan uppnås genom mikroresonatorer som drivs av en laser, vilket ger ultrakorta ljuspulser med en bred spektral bandbredd.

I denna avhandling analyseras linjära interferometritekniker som använder frekvenskammar, särskilt konfigurationen med dubbla frekvenskammar. Genom att använda två frekvenskammar tillåter denna teknik spektropskopisk mätning av ett prov med hög upplösning och korta mättider. Intresset för att implementera denna teknik med hjälp av mikrokammar har väckt stort intresse, men förverkligandet är fortfarande utmanande.

I denna avhandling studeras dynamiken i generering av mikrokammar och deras inverkan på deras spektrala egenskaper. Specfikt demonstreras olika metoder för att stabilisera genereringen, vilket har gjort det möjligt att för första gången implementera interferometri med dubbla platikonmikrokammar. Dessutom presenteras en metod för att finjustera en mikrokam, något som potentiellt kan används för att övervinna de begränsningar som uppstår från avståndet mellan olika kamtänder.

Dessutom undersöks i avhandligen dynamiken för spektral breddning, och med hjälp av nanofotonikvågledare med ultralåg förlust, uppnås generering av koherenta spektra som är större än en oktav. Sammantaget bidrar resultaten av denna avhandling till att möjliggöra frekvenskammar i chipsskala med omfattande spektral täckning, hög upplösning, hög känslighet och snabba mättider inom området optisk interferometri.

Publications

This thesis is based on the work contained in the following papers:

[A] **I. Rebolledo-Salgado**, Z. Ye, S. Christensen, F. Lei, K. Twayana, J. Schröder, M. Zelan, and V. Torres-Company, "Coherent supercontinuum generation in all-normal dispersion Si_3N_4 waveguides", *Optics Express*, 30, 8641-8651, 2022.

[B] **I. Rebolledo-Salgado**, Ó. B. Helgason, Z. Ye, J. Schröder, M. Zelan, and V. Torres-Company, "Platicon dynamics in photonic molecules", *Communication Physics*, 6, 303, 2023.

[C] K. Twayana[†], **I. Rebolledo-Salgado**[†], E. Deriushkina[†], J. Schröder, M. Karlsson and V. Torres-Company, "Frequency-comb-based spectral interferometry for characterization of photonic devices", *Micromachines*, 13, no 4, p. 614, 2022.

[D] M. Girardi, Ó. B. Helgason, C. H. López Ortega, **I. Rebolledo-Salgado** and V. Torres-Company, "Super-efficient microcombs at the wafer level", *Submitted*, 2023.

[E] **I. Rebolledo-Salgado**, Ó. B. Helgason, V. Durán, M. Girardi, M. Zelan and V. Torres-Company, "Active feedback stabilization of super-efficient microcombs in photonic molecules", *Submitted*.

[F] **I. Rebolledo-Salgado**, V. Durán, Ó. B. Helgason, M. Girardi, M. Zelan and V. Torres-Company, "Thermal-Controlled Scanning of a Bright Soliton in a Photonic Molecule", *Proceedings of Conference on Lasers and Electro-Optics Europe/ European Quantum Electronics Conference (CLEO/Europe-EQEC)*, Munich, Germany, paper ed62, 2023.

[†]Equal contribution.

Related publications and conference contributions by the author, not included in the thesis:

[G] I. Rebolledo-Salgado, Z. Ye, S. Christensen, F. Lei, J. Schröder, M.Zelan, V. Torres-Company "Nonlinear Broadening of Electro-Optic Frequency Combs in All-Normal Dispersion Si_3N_4 Waveguides", *Proceedings of Conference on Lasers and Electro-Optics Europe/ European Quantum Electronics Conference (CLEO/Europe-EQEC)*, 2021, pp. 1-4.

[H] E. Deriushkina, I. Rebolledo-Salgado, M. Mazur, V. Torres-Company, P. Andrekson, S. Gross, M.J Withford, T. Hayash, T. Nagashima, J. Schröder, M. Karlsson "Characterisation of a Coupled-Core Fiber Using Dual-Comb Swept-Wavelength Interferometry" *Proceedings of European Conference on Optical Communication (ECOC)*, 2021, pp. 1-1.

[I] Israel Rebolledo-Salgado, Óskar B. Helgason, Zhichao Ye, Jochen Schröder, Martin Zelan, and Victor Torres-Company, "Photonic molecule microcombs at 50 GHz repetition rate", *Conference on Lasers and Electro-Optics*, San Jose, USA, paper SW4O.8, 2022.

[J] Israel Rebolledo-Salgado, Óskar B. Helgason, Zhichao Ye, Jochen Schröder, Martin Zelan, and Victor Torres-Company, "Linear Broadband Differential Phase Measurement of Soliton Microcombs", *Conference on Lasers and Electro-Optics*, San Jose, USA, paper SW4O.8, 2022.

[K] E. Deriushkina, I. Rebolledo-Salgado, M. Mazur, V. Torres-Company, P. Andrekson, J. Schröder, M. Karlsson "Dual-Comb Swept-Wavelength Interferometry: Theory and Experiment", *Journal of Lightwave Technology*, 40, 19, 6508-6516, 2022

[L] K. Twayana, F. Lei, Z. Ye, I. Rebolledo-Salgado, Ó. B. Helgason, M. Karlsson, V. Torres-Company "Differential phase reconstruction of microcombs", *Optics Letters*, 47, 3351-3354, 2022.

[M] I. Rebolledo-Salgado, Óskar B. Helgason, Marcello Girardi, Martin Zelan and Victor Torres-Company, "Active Feedback Stabilization of Super-efficient Microcombs", *Proceedings of Conference on Lasers and Electro-Optics Europe/ European Quantum Electronics Conference (CLEO/Europe-EQEC)*, Munich, Germany, paper ci22, 2023.

[N] Krishna Twayana, Israel Rebolledo-Salgado, Marcello Girardi, Fuchuan Lei, Óskar B. Helgason, Magnus Karlsson, and Victor Torres-Company, "Multi-heterodyne Differential Phase Measurement of Microcombs", *Proceedings of Conference on Lasers and Electro-Optics Europe/ European Quantum Electronics Conference (CLEO/Europe-EQEC)*, Munich, Germany, paper cfp7, 2023.

Contents

Acknowledgement

This thesis is the fruit of almost five years in which I have been privileged to be supported by a lot of people whom I wish to acknowledge. The first and biggest goes to the most important person in my life, my fiancée Wendy. Her support, love, and kindness always make my days brighter and I am sure that without her I could not have gotten this far.

My immense gratitude to my supervisor Prof. Victor Torres who has given me so much. I will be always thankful for his guidance and patience, especially during my first years. His support, encouragement, and tremendous leadership skills always inspired me to go further. I was very lucky to have Dr. Martin Zelan as my co-supervisor, who has encouraged me from the very beginning and placed so much trust in me. I will be always thankful for his scientific insights, and all his advice about living in Sweden and pursuing my career.

Many thanks to my examiner Prof. Åsa Haglund and to Prof. Peter Andrekson for their insights and for taking care of my academic record. I also thank Dr. Jochen Schröder and Prof. Magnus Karlsson for always answering my questions with great detail. I would also like to express my gratitude to the people at RISE for all their help, especially to my manager Jörgen Spetz who gave me the freedom so I can focus only on my doctoral studies.

I am thankful to have worked closely with the bright and wonderful people members of the Ultrafast Photonics group. Special thanks to my best friend Dr. Marcello Girardi, I will always treasure his company during our PhD journey, and thank him for sharing with me so much knowledge, especially about fabrication. Dr. Zhichao Ye deserves a big acknowledgment because his excellent fabrication made possible much of this work. I also would like to thank Dr. Francisco Artega and Dr. Simon Christensen for all the help and insights on the supercontinuum generation. Dr. Oskar Helgasson also deserves my gratitude for teaching me about microcombs and always making the lab work amenable. I

would also like to express my admiration for Dr. Fuchuan Lei and thank him for sharing all his knowledge and curiosity. I appreciate having Krishna Twayana as my office mate, thanks for all the help and long conversations about science, football, and politics. Big thanks to Yi and Yan for being good colleagues and for all their diligence at work. Also to Carmen, Sara, and Vijay, for being very propositive, efficient, and taking good care of the lab.

I am thankful to all the current and former members of the Photonics lab for creating such a nice environment for work. Especially to Dr. Kovendhan Vijayan, Dr. Ali Mirani, Zonglong, and Rasmus for sharing their knowledge about fiber optics and always being willing to help. I also want to thank Estrella and Sara for sharing with me all their enthusiasm and great company during after-work hours. There is nothing better in the lab than having a good partner. For that, I thank Ekaterina Deriushkina for the experiments we performed together and for always having such a positive attitude, efficiency, and good topics of conversation. I also thank Clara Quevedo for her extraordinary company, brilliance, and dedication, I enjoyed so much working with her. Another big thanks to Dr. Vicente Durán for teaching me a lot and for his excitement every time we made a measurement.

Life in Göteborg has been easier having many amazing friends surrounding me. Many thanks to Ansku for her cheerfulness and for always trying to bring me closer to the Nordic culture. Thanks to Gaby for her friendship and for always pushing me to try new things. Big thanks go to Felix, for his kindness and the bouldering sessions at lunchtime. Ali, Maryam, Roger, Diego, and Pame also deserve my thanks for always making me feel at home.

Finally, I would like to thank my family for all their support and encouragement. Muchas gracias a mi papá y mamá por enseñarme el valor del trabajo y por la educación que me dieron, la cual será mi mejor herencia. I also thank my siblings for all their love, especially my brother Daniel, for being my best friend and always being there for me.

Isra Rebolledo
Göteborg, Sweden
November 2023

Acronyms

DCI	dual-comb interferometry
CW	continuous wave
DKS	dissipative Kerr soliton
EO	electro-optic
IM	intensity modulator
PM	phase modulator
SC	supercontinuum
FSR	free spectral range
SPM	self-phase modulation
OWB	optical wave breaking
MI	modulation instability
FWM	four-wave mixing
GVD	group velocity dispersion
LLE	Lugiato-Lefever equation
Microcomb	microresonator frequency comb
DUT	device under test
MLL	mode-locked laser
OFC	optical frequency comb
RF	radio frequency
FPGA	field-programmable gate array

Chapter 1

Introduction

The spectral nature of light can be readily seen in a rainbow when the rain showers. This occurs when the light from the sun is refracted as it passes through the water droplets in the air. Although this phenomenon has amazed people for thousands of years, the presence of colors was merely a curiosity without any scientific significance. This changed in the 17th century when Isaac Newton realized the separation of sunlight into a series of colors, introducing the concept of a spectrum for the first time. In his experiments, he used an arrangement composed of a lens, a prism, and a screen to analyze the light. The invention of this first spectrograph, and the later work on the observation of dark lines in the solar spectrum made by Wolleston and Fraunhofer, established the beginning of modern spectroscopy [1].

Optical spectroscopy is nowadays a ubiquitous tool in research and industry since it offers methods to characterize samples non-destructively with high sensitivity. Spectroscopy can be realized over the whole electromagnetic spectrum, where the wavelength regions are of different relevance depending on the application. Concretely in optical spectroscopy, the mid-IR and far-IR regions are quite appealing since many chemical substances have vibrational transitions that can be probed directly.

From the early days of spectroscopy, incoherent broadband light sources, such as xenon arc lamps, halogen-based sources, and thermal emitters have been employed since they are cost-effective and very simple to operate [2]. These sources in combination with Fourier-transform (FT) spectrometers have been traditionally used for absorption spectroscopy, i.e. intensity-based spectra measured as a function of the frequency or wavelength [3]. Additional information about the sample under test can

be retrieved by measuring the phase which offers insights into the temporal behavior of the optical field. This can be achieved using spectral interferometry, where the measurement of the amplitude and phase of an unknown sample is possible under the assumption that the light source is known.

1.1 Laser interferometry

The advent of the laser led to a revolution in optical interferometry since it provided an intense source of light with a high degree of temporal and spatial coherence. This, in turn, translates into highly sensitive measurements with high spectral resolution limited in theory only by the linewidth of the laser. These properties have stimulated numerous applications of laser spectroscopy in a wide range of areas, including environmental monitoring, medical diagnosis, chemical analysis, and material science [4, 5]. However, a significant limitation of laser-based spectroscopy lies in the spectral bandwidth of the lasers employed for these applications, e.g. tunable lasers.

At the beginning of this century, a new type of laser called frequency comb, initially developed for metrology, has proven to be an excellent source for optical spectroscopy [6, 7]. The unique feature of frequency combs is that they possess broad spectral emission composed of discrete evenly-spaced laser lines. Thus, applied to spectroscopy, they combine a large spectral span (a distinctive characteristic of FT spectroscopy using incoherent sources) with the narrow linewidth resolution and high intensity offered by laser spectroscopy [8]. Furthermore, the most significant advantage of frequency combs for spectroscopy is the possibility of calibrating the frequency scale with high accuracy, enabling the comparison of measurements between laboratories around the world.

The use of frequency combs has been applied to an extensive number of applications including biochemical environmental sensing [9], human breath analysis [10], gas absorption spectroscopy [11, 12] and astronomy [13]. These implementations have leveraged frequency combs in various spectroscopy configurations utilizing their different properties which can be roughly characterized by spectral coverage, sampling, and resolution.

Spectral coverage. Depending on their architecture, frequency combs can extend over large optical spans, in some cases, covering multiple frequency octaves [14]. The coherent nature of frequency combs is portrayed as a train of pulses in the time domain, where the pulse duration

reduces as the optical bandwidth increases. This provides a high resolution in time, making them extremely useful for measuring ultrafast phenomena. At the same time, their spatial resolution given by their pulse duration is typically in the order of micrometers which is useful for microscopy applications. The optical bandwidth and region of emission of the frequency comb typically depend on its gain medium, and by employing nonlinear frequency conversion it is possible to increase the frequency span and access spectral regions of challenging direct emission such as the mid-infrared [15]. In this regard, the near-infrared region is perhaps the most mature technology in terms of coherent spectral sources fueled by telecommunication applications. Although vibrational overtones coming from molecular phenomena can be measured in this region, equally important is that the methods developed and tested in the near-IR, can in principle be applied to longer wavelengths.

Spectral resolution. The linewidth of the frequency comb lines can be extremely narrow, often in the order of a few hertz to kilohertz. This is a direct consequence of the high degree of phase coherence among the comb lines. Frequency combs can be frequency stabilized to sub-Hertz linewidth lasers which allows to transfer of their low noise properties to the comb lines [16]. Narrow linewidth offers the possibility of defining spectral features with high precision, however, it is necessary to resolve the individual lines of the frequency comb.

Spectral sampling. Although the spectral resolution is imparted by the linewidth of the frequency comb when probing a sample, due to its discrete nature, the measurements are performed at the frequency of the repetition rate of the comb. Depending on the comb platform, the spectral sampling can be in the order of hundreds of MHz to tens of GHz. Therefore, the repetition rate of the comb should be chosen as a function of the type of sample to be measured. In most cases, the comb spacing is usually a parameter fixed by construction, directly related to the length of the cavity where the comb is generated. Thus implying a trade-off between the compactness of the frequency comb and its spectral sampling.

1.2 Miniaturization of spectrometers via integrated photonics

1.2.1 Dispersive and interferometric microspectrometers

In the previous section, the basic properties of the frequency comb were presented, but equally important for performing spectroscopy are the instrumental schemes. Ultra-high resolution measurements are attainable with modern spectrometers, for example, based on dispersive elements. In traditional grating-based designs, the light is spatially separated and projected onto a photo-detector array. Another approach is using Fourier-transform (FT) spectrometers based on scanning interferometric systems [3, 17]. Using such a configuration, an optical signal is split into two optical paths, one with a different length which will cause a temporal delay. The two arms are then combined and an interference pattern is obtained from the superposition of the original optical signal with its delayed copy. This type of spectrometer can record well-resolved spectra, however, it requires long-distance scanning ranges.

These conventional setups can deliver outstanding performance but they rely on large instrumental setups due to the inherent relation between resolution and optical path length. Some applications such as industrial monitoring processes, medical diagnosis [18, 19] or food quality monitoring [20] do not require ultra-high resolution, but instead need compact systems that can perform on-spot measurements. Thus, a trend towards the miniaturization of spectrometers has emerged during the last decade. The miniaturization of spectrometers can enable portability, reduction of footprint, lower power consumption, and wafer-scale fabrication [21]. There is also an increased interest in embedded micro spectrometers on smartphones for bio-sensing which can take advantage of the data processing power of mobile computing [18, 22].

Many approaches have investigated the possibility of mimicking the bench-top strategy based on dispersive and interferometric techniques [23–25]. Several demonstrations of on-chip spectrometers have been reported using photonic integrated circuits such as waveguides and gratings to perform a similar task as free-space optics components [26–28]. For example, using arrayed waveguide gratings to build dispersive spectrometers. However, the trade-off between the footprint size and resolution still remains [29–31]. Additionally, the dispersive configuration suffers from high signal-to-noise ratio penalties due to the spreading of light into different channels and is also more vulnerable to fabrication errors

that can produce cross-talk among the channels.

The integration of FT spectrometers has been also shown using integrated planar platforms [25, 32, 33]. In traditional FT spectrometers, the movement of mirrors is performed to tune the optical path length. In planar technologies such as silicon photonics, this is achieved using a thermo-optic modulation effect, or employing arrays of discrete integrated interferometers [34, 35]. Fourier transform spectrometers, benefit from a multiplexing advantage where many spectral components are measured simultaneously.

The reduction of spectrometers inevitably poses a challenge due to the competing requirements in terms of size and performance. Although boosted SNR and high resolution are now possible, reducing the chip footprint is an ongoing topic of investigation regarding the scalability of dispersive and FT spectrometers. A path towards mass-scale production is the use of silicon photonics, enabled by lithography-based fabrication and its compatibility with CMOS technologies.

1.2.2 Chip-scale dual-comb spectrometers

The advances of photonic integration have also provided a route towards the miniaturization of frequency combs and their mass-scale manufacturing [36]. The accessibility of high-performance frequency combs has significantly contributed to the appeal of a comb-enabled spectroscopy technique, the dual-comb spectrometer. This scheme is based on the Fourier-transform approach but replaces the moving components with a second frequency comb. The evolution of integrated frequency comb technology has enabled the realization of dual-comb spectroscopy using chip scale devices based on semiconductor materials [37–39] and nonlinear frequency generation [40–43].

Semiconductor gain materials have attracted significant attention for the realization of integrated frequency combs emitting in the mid-infrared and terahertz frequency regions. Some of their key advantages are wafer-scale fabrication, electrical pump operation, and by engineering the semiconductor band-gap is possible to tailor the wavelength region emission [39, 44]. These integrated sources of radiation have shown to be suitable to perform dual-comb spectroscopy with similar performance as conventional fiber-based systems [37, 39, 45]. Nevertheless, an important trade-off of this technology is the frequency bandwidth limited by the material gain.

Frequency combs can be also generated in nonlinear media pumped

with continuous wave lasers. Depending on the type of nonlinearity of the medium, the generated frequency combs exhibit different spectral characteristics [36]. Integrated nonlinear frequency combs rely on the ability to strongly confine the modes in a waveguide to harness nonlinear effects. The first demonstrations were made based on Kerr nonlinear microresonators [46], since then the research field has been very active during the last decade. An important characteristic of Kerr nonlinear combs is that their gain bandwidth is not limited by the material but instead can be tailored by waveguide geometry, giving excellent design flexibility. In addition to Kerr comb generation, other integrated frequency combs based on electro-optic effects [47, 48] and wave-nonlinear interaction have gained significant attention.

Indeed, the generation of Kerr combs has been explored in different material platforms that offer high nonlinearities and the possibility of dispersion engineering. However, silicon nitride has become a successful platform for integrated photonics since it possesses a large transparency window (0.4 μm - 4μm) [49], this is appealing for spectroscopy as it can cover regions of interest such as visible and mid-infrared. Furthermore, silicon nitride stands out due to its compatibility with CMOS processes and planar fabrication [50, 51]. On-chip nonlinear Kerr combs have exploited the attainable broad spectral bandwidth and coherence to realize dual-comb spectroscopy in the near-infrared region [40, 41]. Recent works have also demonstrated the use of these combs in a dual-comb interferometry configuration for ranging measurements [52–54]. These demonstrations allow us to envision mass-scale fabricated comb-based spectrometers entirely integrated on a single chip that can be employed in industrial applications.

1.3 This thesis

This thesis focuses on the study of the generation of chip-scale frequency combs to extend its capabilities to broadband optical spectroscopy. The chip-based frequency combs are realized through supercontinuum generation (SCG) in optical waveguides and Kerr-comb generation in microresonators. The research is framed around the challenges of realizing chip-scale dual-comb spectrometers such as coherence and long-term stability. Different interferometry techniques based on established frequency comb sources were analyzed to provide insights into comb-spectroscopy in the frequency and time domain. Ultimately, phase-sensitive dual-comb

spectroscopy is demonstrated using on-chip Kerr combs over a broad spectral range in the near-infrared region. As a step towards broadband ultra-high resolution spectroscopy, a method for tuning microcombs is proposed that can potentially mitigate the coarse spectral sampling inherent to microcombs.

In paper A, we proposed the supercontinuum generation implemented in the silicon nitride platform due to the high nonlinear coefficient and the absence of nonlinear absorption losses. The study is focused on the operation in the all-normal dispersion regime as it allows the coherent broadening of spectra using frequency combs with a high repetition rate. An extensive investigation of the coherence properties of the broadened spectra is also performed.

An important challenge in frequency comb generation using microresonators is the usable power per comb line achieved. Microcombs generated in cavities that exhibit normal dispersion offer a high conversion efficiency, meaning an enhanced high signal-to-noise ratio for interferometric measurements. In paper B, the generation of microcombs in the normal dispersion regime using a mode-coupling interaction for the initiation is explored. The effects of mode-coupling interaction and its implications on the spectral characteristics of the microcomb were also studied. Furthermore, we realize dual-comb interferometry for the first time using normal dispersion microcombs.

The integration of this technology offers the possibility of realizing chip-scale spectrometers that cover broad spectral bandwidths with a resolution given by the linewidth of the comb teeth. The implications of frequency combs for linear spectroscopy techniques are also provided as part of this study [paper C].

In paper D, as part of an extensive study on wafer-scale fabrication of microcombs, the demonstration of tri-comb interferometry for broadband phase-sensitive spectroscopy is performed. This work, shows the enabling possibilities of space multiplicity, as a large number of microcombs with similar spectral characteristics were fabricated. Combined with low power consumption, the use of dual-comb spectrometers for multiple sensing points is demonstrated.

A stable operation of microcombs is necessary to perform not only spectroscopy but most of the system-level applications. In paper E, an active control method is presented using a simple approach to stabilize the detuning of the continuous wave laser pumping the microresonator. This approach is also leveraged in paper F, where the

tuning of a microcomb is demonstrated maintaining a low-state noise. The controlled tuning of a microcomb can be employed to increase the spectral sampling in comb spectroscopy hindered by its repetition rate.

Thesis outline

In Chapter 2, the general description of frequency combs is provided along with the different mechanisms to generate them. Chapter 3 revolves around the Kerr microcomb generation using nonlinear nanophotonic waveguides. Chapter 4 focuses on dual-comb interferometry, its applications, and challenges employing high repetition rate frequency combs. In Chapter 5, an overview of the characterization techniques of microcombs and their stabilization is provided. The future outlook of the research work is presented in Chapter 6. Finally, a summary of the papers is presented in Chapter 7, where my contributions are mentioned in detail. Following, two appendices are included which include a detailed schematic to perform dual-comb interferometry using microcombs (Appendix A) and the steps followed to couple free-space light into a waveguide (Appendix A). The appended papers are at the end of the thesis.

Chapter 2

Optical frequency combs

In this chapter, a general description of frequency combs is provided along with the different mechanisms to generate them. Particular attention is given to high-repetition-rate frequency combs, as they have been employed in this research study. Their integration and applications with a central focus on comb-based spectroscopy are also discussed.

2.1 General description of frequency combs

Since the first realization of the laser, it was realized that full control over its frequency would enable a large number of possibilities in science and technological applications. However, the challenge of measuring its absolute frequency was immediately evident as the frequencies were too high to be measured directly. This sparked massive efforts to develop clockworks that could enable measuring the frequency of coherent light. For this purpose, a method proposed was to use harmonic frequency chains based on a stable 100 MHz reference which was multiplied over a large factor to reach optical frequencies. Although this scheme enabled the measurement of visible light, it required a large complex setup with the size of an entire facility and it could only measure a single optical frequency [55]. The advent of a self-referenced frequency comb greatly simplified the measurement of light as it provided a bi-directional connection between the radio-frequency and optical domains [56]. This technology was later recognized with half of the Nobel prize in 2005 [6,7].

An optical frequency comb can be defined as a laser source that emits a series of narrow frequency lines that are equally spaced by its repetition rate (f_{rep}). In the time domain, its output consists of a pulse train with

a constant period, given by the inverse of the repetition rate frequency ($1/f_{\mathrm{rep}}$). Likewise, the frequency comb can be assumed to be a source of pulses with a carrier frequency (f_c) modulated by a pulse envelope $A(t)$. Mathematically, this can be represented as a Fourier series, where the electrical field of the comb is:

$$E(t) = Re(A(t)\exp(i2\pi f_c t)) = Re(\Sigma_n A_n \exp(i(f_c + n f_{\mathrm{rep}} t)), \quad (2.1)$$

where A_n are the Fourier components of $A(t)$ and f_{rep} is the repetition frequency of the comb. Given that f_c is not necessarily an exact multiple of the repetition rate, the spectral lines of the comb are all shifted by a common offset frequency f_0. The frequency comb can then be fully described if the carrier-envelope offset frequency (f_0) and the repetition rate are known. Hence, the absolute optical frequency of each comb line (f_n) is represented by:

$$f_n = f_0 + n f_{\mathrm{rep}}. \quad (2.2)$$

Commonly known as the comb equation, Equation 2.2 illustrates that with the knowledge of these two frequencies, any optical frequency of the comb can be precisely and accurately identified based on f_0 and f_{rep} [57,58]. Measurement of these frequencies with sufficiently high accuracy, provided a straightforward conversion from a microwave frequency to an optical frequency with a multiplication factor n (typically falling within the range of $10^5 - 10^6$).

Different frequency comb platforms have been developed providing astonishing levels of stability and precision, nevertheless, the knowledge of f_0 will be always a key ingredient in the pursuit of absolute accuracy. In the following, an MLL laser, which was used in the first realization of f_0 and f_{rep} control will be used as an example to provide a better grasp of the frequency comb structure.

2.1.1 Mode-locked lasers

Mode-locking is an important concept in frequency comb technology and refers to the process in which a self-organization of different optical frequencies in a cavity allows the generation of pulses. The foundations of frequency combs can be traced back to 1960, with the experimental demonstration of an active mode-locked laser (MLL) using a Q-switching

method [59]. This technique utilized an active modulation of the internal losses of the cavity to control the Q-factor of the resonator. A passive scheme of mode-locking was later proposed replacing the modulators with a fast saturable absorber [60]. A diagram of a MLL setup using a passive scheme is depicted in Figure 2.1 (a).

Later work employed the Kerr-lens effect to achieve mode-locking using a titanium-sapphire crystal as the gain medium [61]. Titanium-sapphire lasers became the most widespread configuration as they provide wide spectral bandwidths in the form of femtosecond pulses. Nevertheless, these mode-locking techniques did not include active feedback stabilization and as a consequence, a dephasing of the pulses occurred due to perturbations in the cavity. It was later shown that active control of the carrier-envelope phase using a self-referencing method will enable absolute optical frequency metrology [62, 63]. Nowadays, mode-locked lasers are an established technology for frequency comb generation. Their optical bandwidth is given by the gain of the rare-earth doped material, usually covering tens of nanometers (see Figure 2.1 (b)).

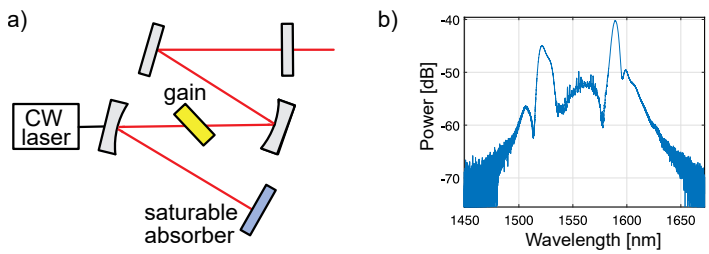

Figure 2.1: Mode-locked laser. (a) The basic setup of a mode-locked laser, where a gain medium is placed in the cavity and a saturable absorber mirror is used to achieve passive mode-locking. (b) The measured spectrum of a femtosecond mode-locked laser from Menlo systems, the spectral envelope is not resolved by the optical spectrum analyzer and appears to be continuous due to the low repetition rate of 250 MHz.

The repetition rate (f_{rep})

This frequency corresponds to the space between two consecutive comb lines. In the time domain, its output is a series of consecutive pulses with a time separation T_r related to the length of the laser cavity that

can be expressed as follows:

$$T_r = \frac{1}{f_{\text{rep}}} = \frac{L}{\nu_g}, \tag{2.3}$$

where f_{rep} is the repetition rate of the frequency comb, L is the length of the cavity, and ν_g is the group velocity of the pulse. This relationship indicates the dependence of the repetition rate with the optical cavity length. It is also evident that variations in the cavity length will have a direct impact on the repetition rate and the pulse-to-pulse time.

The output pulses of the mode-locked laser are conformed by massive amplitude modulation of the frequency carrier by all the spectral components of the frequency comb. This means that all the optical modes interfere with each other to form a pulse, the larger the number of frequency components the shorter the pulse it is. The direct photodetection of these pulses will produce a large number N of frequency harmonics of the repetition rate. However, it does not provide information on the offset frequency, which is common for all of the comb modes. For example, considering the beating of two frequency comb lines (m and n), the beat note measured will yield information on the repetition rate only, i.e.,

$$\nu_m - \nu_n = (f_0 + m f_{\text{rep}}) - (f_0 + n f_{\text{rep}}) = (m - n) f_{\text{rep}}. \tag{2.4}$$

In the case of a fiber-based MLL, the control of the repetition rate frequency can be easily performed since it can be measured using a sufficiently fast photo-detector. Its frequency stabilization can be realized by active feedback to the laser cavity length.

The offset frequency (f_0)

As mentioned before, a key feature of a frequency comb is the ability to measure and control its offset frequency (f_0) enabled through self-referencing. The direct detection of f_0 is extremely difficult since it is related to the phase of the optical carrier. In an MLL, this arises due to the fact that the pulses coming out are not fully identical due to dispersion in the cavity. Instead, a phase shift $\Delta\phi = 2\pi f_0 / f_{\text{rep}}$ between the peak of the envelope and the nearest peak of the carrier wave occurs as shown in Figure 2.2 (a). This phase variation $\Delta\phi$ evolves from pulse to pulse and translates in a frequency shift f_0 of the complete comb (Fig. 2.2 b).

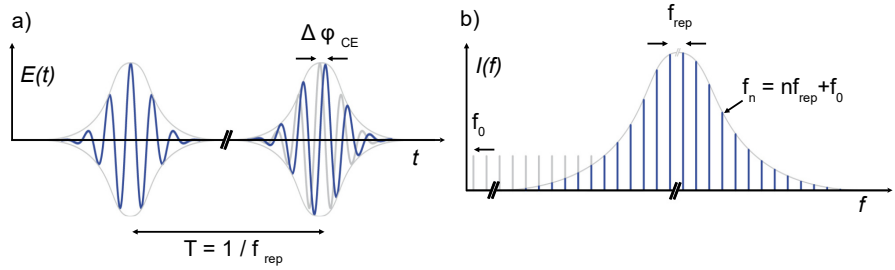

Figure 2.2: (a) Time-domain representation of an optical frequency comb. (b) In the frequency domain, the OFC consists of a broad spectrum of equally spaced comb lines, whose optical frequencies are given by $f_n = nf_{\mathrm{rep}} + f_0$.

In order to assess f_0 directly, one would need to measure the oscillations of the carrier, which is simply not possible with the existing technology.

2.1.2 Self-referencing

A method to determine the offset frequency was proposed in [62,64] using a nonlinear conversion method. This technique, called self-referencing, uses a $f-2f$ interferometer and requires that the bandwidth of the frequency comb spans at least one octave. This was achieved using a highly nonlinear fiber, called photonic crystal fiber [62, 65, 66]. A schematic of the self-referencing method using a broadened frequency comb spanning an optical octave is shown in figure 2.3. In a $f-2f$ interferometer, a comb mode in the low-frequency side is doubled using a nonlinear crystal and interfered with a comb mode that is twice the frequency, providing a frequency beat note as:

$$2(nf_{rep} + f_0) - (2nf_{rep} + f_0) = f_0. \tag{2.5}$$

Achieving self-referencing does not rely exclusively upon second harmonic generation but other nonlinear effects can be employed. It is for example possible to measure f_0 using $(n-1)f-nf$ schemes such as the 2f-3f approach where only two-thirds of an octave are required [67]. In fact, these schemes have been employed with Kerr nonlinear frequency combs, relaxing the requirements of the spectral broadening needed for self-referencing [68].

The control of the degrees of freedom of the optical frequency comb

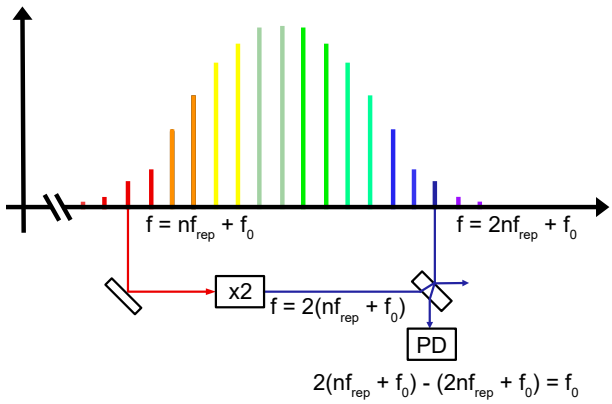

Figure 2.3: Self-referencing technique using a $f - 2f$ method. A mode n at the red side of the spectrum is frequency doubled using a nonlinear crystal. If the frequency comb covers a full optical octave span, a mode $2n$ with a frequency $2nf_{rep} + f_0$ is located on the blue side- The beat note between the doubled-frequency mode and the $2n$ yields the offset frequency.

discussed so far widely enhanced the capabilities of precision metrology. These applications ranged from atomic clock comparisons [69, 70] to molecular spectroscopy [71]. However, not all applications require absolute frequency stability but rather flexibility in the repetition rate tuning and higher power per line. In the following section, other comb generators and their capabilities will be discussed.

2.2 High-repetition-rate optical frequency combs

2.2.1 Electro-optic frequency combs

Electro-optic (EO) frequency combs stand out from other frequency comb generators because of their repetition rate tunability, high optical power handling, and stable operation [72, 73]. They are based on electro-optic modulation. In short, a CW laser is modulated by a microwave signal such that sidebands are generated in the laser spectrum, in which the central and repetition frequencies are defined by the frequency of the laser and the modulation frequency, respectively. These two parameters can be chosen freely within the operation bandwidth of

the modulators, providing a simple yet powerful technique to generate a comb.

Generation

Several configurations of electro-optic combs have been implemented with the purpose of obtaining flat spectral envelopes, which are appealing for spectroscopy and communication applications. In this section, a configuration using cascaded phase and intensity modulators will be discussed since this approach has been employed for the work presented in paper A.

The modulators work utilizing the Pockels electro-optic effect where the refractive index varies in the presence of an electric field. We can start considering a single phase modulator, where the strong phase-modulation imparted on a CW laser will result in a periodic chirp of the light. This means that the modulator simply varies the phase in proportion to the driving voltage, which is generally a sinusoidal electrical waveform with a frequency ω_m. Thus, the optical field of the modulator can be described as:

$$E(t) = A_0 \exp(i\omega_c t + i\Delta\phi \sin(\omega_m t)), \tag{2.6}$$

where A_0 and ω_c are the amplitude of the modulation signal and the carrier frequency. The factor $\Delta\phi$ is the so-called modulation index equal to $\pi V/V_\pi$, which relates the voltage of driving RF-signal, V, with the half-wave voltage of the modulator, V_π. The latter determines the electrical power required to achieve a π-phase change. The ratio between these two parameters must be maximized in order to achieve a broad optical spectrum. In practice, the RF power is limited and the V_π is intrinsically limited by the waveguide structure and electro-optic coefficient of the modulator.

In order to extend the optical bandwidth of the EO comb, it is common to employ a series of N phase modulators [74]. The price to pay using such a scheme is a linear increase of the optical insertion loss with each modulator. Additionally, the temporal phase between the modulators must be carefully aligned using electrical phase shifters. This EO comb configuration is depicted in Figure 2.4 a, where an additional intensity modulator is located at the output of the comb for flattening the spectrum. The intensity modulator should be biased to provide a train of pseudo-square pulses. If this temporal signal is correctly aligned with

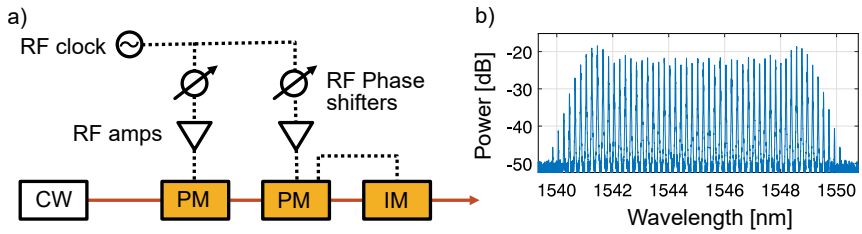

Figure 2.4: a) Electro-optic comb generation using phase and intensity modulation. The cascaded configuration of the two phase modulators (PM) increase the effective modulation depth, while the intensity modulator (IM) flattens the optical spectrum. b) Optical spectrum measured at the output.

the phase of the modulators, the pulses coming out will exhibit a linear phase and hence equalize the spectrum [75]. With this configuration, one usually can get a bandwidth of $\sim$ 1 THz, with such bandwidth the phase noise performance is only limited to the pump laser linewidth since minimal degradation from the RF-clock purity has been found [74, 76].

Spectral broadening

Although it is straightforward to extend the optical bandwidth in a configuration with cascaded modulators, it is inconvenient as it will scale the number of modulators and RF components. A common method to enhance the optical bandwidth is using high-nonlinear fibers. Demonstrations of electro-optic combs broadening to tens of nanometers while maintaining the comb structure have been reported by exploiting soliton compression in anomalous dispersion fibers [73, 77, 78]. An alternative is to broaden the spectra using normal dispersion fibers or waveguides as will be discussed in detail in Chapter 3. The dispersion regime where the fiber operates is of significant importance in order to avoid the decoherence of the pulses as a result of the amplification of input noise.

EO combs have been spectrally broadened to bandwidths that span over an octave to enable self-referencing [79]. For such large broadening, the phase noise accumulation should also be considered in order to maintain the coherence as it increases with respect to the line number [80]. Self-referencing using EO combs, has been demonstrated using a two-stage process to realize such broadening where an initial broadening is performed mainly using a self-phase modulation mechanism operating at a low dispersion. In the second stage, the chirp of the pulse is com-

pensated and coupled to either a fiber or a waveguide that has been dispersion-engineered to perform a large broadening [79, 81]. In [79], the phase noise was mitigated using a microwave cavity in a stabilized-local-oscillator configuration, diminishing the comb linewidth broadening far from the central frequency. Equally important was the use of an optical cavity (with a free spectral range matched to the comb repetition rate) to filter out the optical phase noise.

2.2.2 Integrated architectures

The electro-optic frequency comb generator previously described is an established technology that employs bulk lithium niobate modulators [72–74]. A similar output spectrum has been realized leveraging the thin-film lithium niobate on insulator (LNOI) platform showing a high performance in terms of optical propagation loss and driving voltage [82, 83].

Similar to EO combs, micro-resonators generate a frequency comb starting from a CW laser. However, the principle is completely different. The generation of a microcomb is based on the resonant re-circulation of light that allows the build-up of optical power to harness the non-linearities of the medium. The first demonstrations of microcombs were based on whispering gallery mode resonators and have spread over a large number of fabrication technologies and materials [84, 85]. As the focus of this thesis is centered around microcombs, a detailed explanation will be given in the next chapter.

Other platforms such as semiconductor gain materials are appealing for the realization of coherent frequency combs in a wafer-scale production. Integrated mode-locked lasers can be generated in quantum well (QW) structures or quantum dot materials (QD) in order to generate short pulses in visible and near-infrared wavelengths [86–90]. Based on quantum wells, quantum cascade lasers are another attractive solution to generate combs in the mid-infrared and the terahertz region [44, 91, 92]. Indeed, the field of integrated platforms has advanced rapidly, and the reader looking for details can find them in excellent sources in the literature [36, 93].

2.2.3 Applications

Frequency combs with high repetition rates are appealing to applications such as communications, astronomy, and RF photonics, they are

less demanding in terms of bandwidth and absolute stabilization but instead, the frequency spacing plays a more important role [13, 72, 94]. In astronomy, a frequency comb is superimposed with the observed light collected using a spectrograph, providing an accurate calibration of the wavelength scales [95]. A challenge for this application is that the adjacent comb modes should be easily resolved from one to another, the initial demonstrations made use of an MLL filtered by a Fabry-Perot cavity to increase the effective mode spacing. These sources referred to as astrocombs, are now realized using electro-optic combs or microcombs that provide directly a wider comb spacing eliminating the need for complex filtering setups [96–98].

In optical communications, wavelength division multiplexing (WDM) is a successful technology where OFCs can be exploited as optical carriers that can be modulated and transmitted, potentially replacing hundreds of lasers with a single unit. The spacing of the optical channels is standardized by the International Telecommunication Union (ITU) typically in 25, 50, and 100 GHz. This channel spacing can be delivered by electro-optic and Kerr nonlinear frequency combs which have proven to be a robust and compact alternative in modern communications [94, 99, 100].

Another communication technology is RF photonics, where the main incentive is to provide functionalities to microwave systems that are impossible due to their limitations in bandwidth [72]. One example is the generation of arbitrary waveforms using pulse shaping methods, this requires a frequency comb at a high repetition rate in order to match the resolution of the available shapers [101]. This technique has been used in paper A to compress the output pulses of an electro-optic comb and in papers B and D to program a phase filter across the optical spectrum of a microcomb.

Uses for spectroscopy

Although having a low repetition rate comb (in the MHz range) is desirable for spectroscopy as it increases the spectral sampling resolution, working with repetition rates in the GHz range is particularly suitable for applications where dynamic measurements are needed. For example, using a single comb for molecular spectroscopy, in [102] cesium transitions were probed with the pulses of an EO comb which provided a microsecond scale of measurements. Other studies on atomic spectroscopy have also benefited from the flexibility of the tuning of the line spacing to achieve rapid temporally resolved measurements [103, 104].

By using two frequency combs, dual-comb spectroscopy (DCS) has aroused the highest interest due to its performance capabilities in terms of SNR and fast measurements. EO comb generators are very attractive for dual-comb spectroscopy since they significantly reduce complexity compared to MLLs-based systems. Several demonstrations for gas spectroscopy have been reported using this configuration [105–107]. Although the large spectral sampling given by the repetition rate could be detrimental, it allows to have a high refresh rate of measurements [108–110]. Microcombs are also very attractive to implement this configuration since they represent an opportunity to reduce component size and complexity in a myriad of outside laboratory applications [40,53,54,111].

DCS on-chip has been demonstrated in the near-IR region where most of the microcomb demonstrations have been focused [112–115]. Demonstrations in the mid-infrared have also been realized in the wavelength range from 2.6 μm to 4.1 μm in the silicon platform [42]. Other approaches to perform DCS in the mid-IR region with GHz sampling resolution involve the use of a nonlinear crystal [43] to convert from a near-IR microcombs to the mid-IR region [116]. The dual comb technique, demonstrated in papers B and D will be covered in more detail in Chapter 4.

Chapter 3

Chip-scale frequency combs with nonlinear nano-photonic waveguides

Integrated photonics has enabled the generation of frequency combs at the chip scale. Photonic devices implemented within square millimeter areas are capable of providing high confinement which is essential for nonlinear optics. Similar to the first realizations utilizing fiber optics, they enable the possibility of tailoring the dispersion profiles to further enhance the nonlinear parametric processes.

In connection with the results presented in papers A and B, this chapter is mainly focused on the generation of nonlinear broadened spectra and microcomb generation in the normal dispersion regime. The influence of the pulse duration on the coherence of supercontinuum generation will be analyzed. At the end of the chapter, insights into the generation of microresonator frequency combs will be provided.

3.1 Nonlinear optics in waveguides

The generation of broadband spectra on chip typically relies on supercontinuum (SC) generation through Kerr nonlinearity in optical waveguides and microresonators [117]. A notable distinction between SC and Kerr frequency comb generation lies in their respective pump sources. SC generation employs a pulsed source, while Kerr comb generation is driven by a continuous-wave (CW) laser. As the pump pulse itself is a frequency comb in SC generation, the repetition rate of the input pulse is main-

tained in the broadened spectra. Conversely, in Kerr comb generation, the CW laser couples to one of the microresonator resonances, transferring energy to other cavity modes via four-wave mixing (FWM), with the repetition rate defined by the free spectral range of the microresonator.

In both approaches, achieving high confinement and engineering the dispersion is made possible through the manipulation of the waveguide geometry, crucial for enabling nonlinear optics processes. [118]. When using a straight waveguide, the propagation length is another critical parameter to be considered.

3.1.1 Supercontinuum generation

As discussed in previous chapters, laser spectroscopy can be realized in different regions of the spectrum depending on the target specimen. That has motivated the development of new material platforms that can lase at different wavelengths. A particularly effective means to effectively generate a wide range of wavelengths is supercontinuum generation. This process relies on the nonlinear broadening of narrow-band pulses creating a continuous output spectrum and was first observed in glass material [119]. Decades later, the emergence of photonic crystal fibers (PCF) opened new opportunities by facilitating the engineering of modal confinement, nonlinearity, and dispersion [65]. Subsequently, supercontinuum generation in fibers has been heavily studied, and the methods developed have found applicability in integrated photonic waveguides as well.

In the last decade, the generation of on-chip supercontinuum has been explored in various material platforms such as silicon [120, 121], silicon nitride [50, 122, 123], AlGaAs [124], and AlN [125]. Silicon nitride is advantageous due to its wide transparency window, high nonlinear coefficient, and absence of nonlinear losses like two-photon absorption in the near-infrared. The results presented in this thesis have been obtained using waveguides fabricated in Si_3N_4, nevertheless, the methods that will be discussed can be also applied to other material platforms.

The governing nonlinear mechanisms differ based on the dispersion regime of operation of the waveguide, leading to variations in the achievable spectral broadening bandwidth and coherence [126]. Additionally, these properties are influenced by the characteristics of the pulse injected into the guided mode of the optical waveguide. It's crucial for the pulse to have enough energy to initiate nonlinear interactions, and its evolution will depend on the dispersion and nonlinearity characteristics of the

waveguide.

In a dispersive medium, the pulse will be affected by the frequency-dependent propagation constant, β which causes different frequencies to travel at different velocities. The dispersion in the optical mode results from both material and waveguide dispersion. The propagation constant can be expressed as a Taylor expansion,

$$\beta(\omega) = \beta_0(\omega_0) + \beta_1(\omega - \omega_0) + \sum_{n=2}^{\infty} \frac{\beta^n}{n!}(\omega - \omega_0)^n, \tag{3.1}$$

where β_n represents the nth-order derivative with respect to the angular frequency ω, and β_1 is associated with the group velocity $\nu_g = 1/\beta_1$. The second-order derivative β_2, characterizes the group velocity dispersion (GVD) coefficient. When $\beta_2 > 0$, the waveguide features normal dispersion, meaning that the low-frequency components travel faster than the high-frequency components and vice versa for anomalous dispersion which occurs when $\beta_2 < 0$. While dispersion is a linear phenomenon, it significantly influences the nonlinear interactions of the waveguide by affecting the phase-matching condition during spectral broadening.

To describe the pulse propagation through a Kerr nonlinear waveguide, the nonlinear Schrödinger equation (NLSE) is employed. Simulating this equation can be achieved through a split-step method approach, considering the propagation in small steps, accounting separately for the linear and nonlinear terms of the NLSE [127].

$$\frac{\partial A}{\partial z} = -\frac{\alpha}{2}A + \frac{i\beta_2}{2}\frac{\partial^2 A}{\partial t^2} + i\gamma|A|^2 A. \tag{3.2}$$

In the NLSE, the change of the slowly varying electric field envelope (A) with respect to the propagation distance is related to the Kerr nonlinear effect, the GVD, and the propagation losses, as seen on the right side of Equation 3.4 respectively. For simplicity, β_1 is usually removed from the simulations and a co-moving frame at the group velocity is considered. The Kerr nonlinearity in the NLSE is represented by the nonlinear parameter γ, which causes a change in the refractive index of the mode resulting in an intensity-dependent phase.

It is clear that in order to describe the evolution of a pulse in a nonlinear medium, the dispersion and the nonlinearity must be examined together. In the case where the waveguide features normal dispersion, the combination of GVD and self-phase modulation (SPM) produces a broadening of both the spectrum and the pulse. In the presence of

anomalous dispersion, the nonlinear frequency chirp is balanced with the GVD which in turn enables the generation of solitons. Indeed, soliton-induced dispersive wave generation represents an efficient option for SC generation. However, these processes rely on a region of parametric gain called modulation instability (MI). A drawback of this method is that unseeded MI-gain can amplify the noise of the input pulse [128], restricting the duration of the pump pulses in order to maintain a coherent spectrum. This hinders the possibility of compressing pulses that are in the picosecond regime, which is the typical width of frequency combs with high repetition rates, such as EO-combs.

3.1.2 Supercontinuum generation in the all-normal dispersion regime

An alternative for coherent SC generation is working in the all-normal dispersion (ANDi) regime where all soliton dynamics are suppressed. Instead, the dominant nonlinear dynamics are SPM and optical wave breaking (OWB) [129]. Although the employment of ANDi fibers has been studied extensively for SC generation, its realization on integrated waveguides is still challenging. There are two key aspects to consider for the realization of nonlinear broadening in the ANDi regime. First, since the maximum broadening is governed by the initial SPM, the pulse should not broaden immediately. Therefore, the GVD should be as low as possible to keep a high peak power. Second, since the OWB distance grows with the duration of the pulse, the propagation distance should be large enough.

In figure 3.1(a) and (b), a simulation of SC generation in the anomalous and the normal dispersion regime is depicted in order to distinguish key differences. The pump pulse employed for the simulations is a transform-limited Gaussian pulse with a duration of 0.8 ps and an energy of 200 pico-joules. The same input pulse is used in both cases and is propagated in a waveguide with a length of 20 cm. Using a waveguide dispersion of -40 $ps^2 \cdot km^-1$, the spectral evolution shows that the spectral broadening is induced by a soliton until it breaks apart after propagation around 10 cm. As a result, the output spectrum exhibits a complex structure with large dips, these spectral variations are undesirable for many applications. The ANDi waveguide is also simulated under the same conditions using a dispersion of 40 $ps^2 \cdot km^-1$. It is clear that the spectral broadening is driven only by self-phase modulation, and it is considerably narrower than the anomalous dispersion case. However,

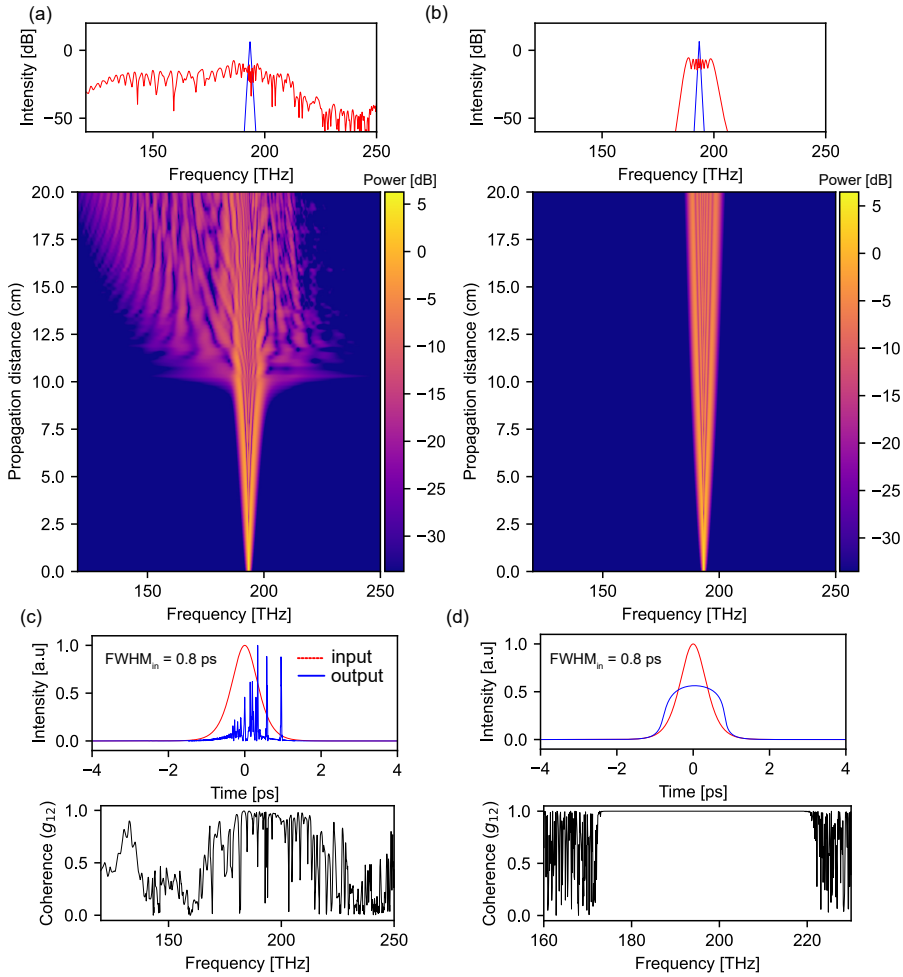

Figure 3.1: Spectral evolution of the SC generation and coherence properties in anomalous and normal dispersion waveguides with a length of 20 cm. (a) an anomalous dispersion waveguide (β_2 = -40 ps^2·km$^-$1) is pumped using a pulse with 0.8 picoseconds duration and 200 picojoules. (b) The same pulse is injected in a waveguide with a β_2 = +40 ps^2·km$^-$1. The temporal coherence $g_{12}(\omega)$ of the anomalous (c) and normal dispersion (d) waveguide was calculated from 20 individual spectra adding shot noise. The input and output temporal profiles of the pulses are plotted on top for each case.

it is important to analyze the coherence properties of the spectrum.

The simulations in Figure 3.1 (a) and (b) correspond to a single pulse

calculation, but the properties of the spectrum can change from pulse to pulse. This arises due to the fact that the input pulse will exhibit a shot noise level which will affect the generated SC. Therefore it is important to analyze the pulse-to-pulse variations, commonly characterized using the spectrally resolved module of the first-order spectral coherence, represented by:

$$g_{12}(\omega) = \frac{|\langle E_j^*(\omega)\rangle E_i(\omega)|}{\sqrt{\langle|E_j(\omega)|^2\rangle\langle|E_i(\omega)|^2\rangle}}, i \neq j, \tag{3.3}$$

where the angled brackets are the averaged spectrum of two different pulses E_i and E_j. This will result in a positive number from 0 to 1. In the anomalous dispersion regime (see Figure 3.1 (c)), using a long pulse causes large shot-to-shot fluctuations, and the coherence is degraded. In contrast, since the noise amplification due to MI is suppressed in the normal dispersion regime, the coherence is maintained which is readily observed as the $g_{12}(\omega)$ is equal to 1 over the whole bandwidth (Figure 3.1 (d)). These comparisons underline the challenges in the spectral broadening of pulses with long durations using waveguides in different dispersion regimes.

Another parameter to consider besides the duration of the input pulse is the energy which is dictated by the average power and the repetition rate. In practice, these parameters might be limited by the maximum optical power of the amplifier and the high repetition rate of the comb. To increase the peak power, hence the nonlinear effects, it is possible to reduce the duration of the pulse up to a certain extent, in paper A, four phase modulators were cascaded to achieve a pulse width of 500 femtoseconds. Under these conditions, a broadening mainly dominated by SPM was still obtained. In order to observe OWB phenomena in the ANDi waveguide it was needed to pump it using pulses with a higher energy.

To examine closely the spectral characteristics of OWB, a pulse in the sub-picosecond regime can be simulated at different propagation lengths as shown in Figure 3.2. Its propagation can be shown using a spectrogram, which displays the time-frequency correlations of the supercontinuum generated. At the initial stage of the pulse propagation (see Figure 3.2 (a)), the spectral broadening is mainly produced by SPM as the characteristic oscillatory structure in the spectrum is observed. In the temporal domain, the pulse maintains its shape and broadens from its initial duration and the spectrogram exhibits a S-shape typical of

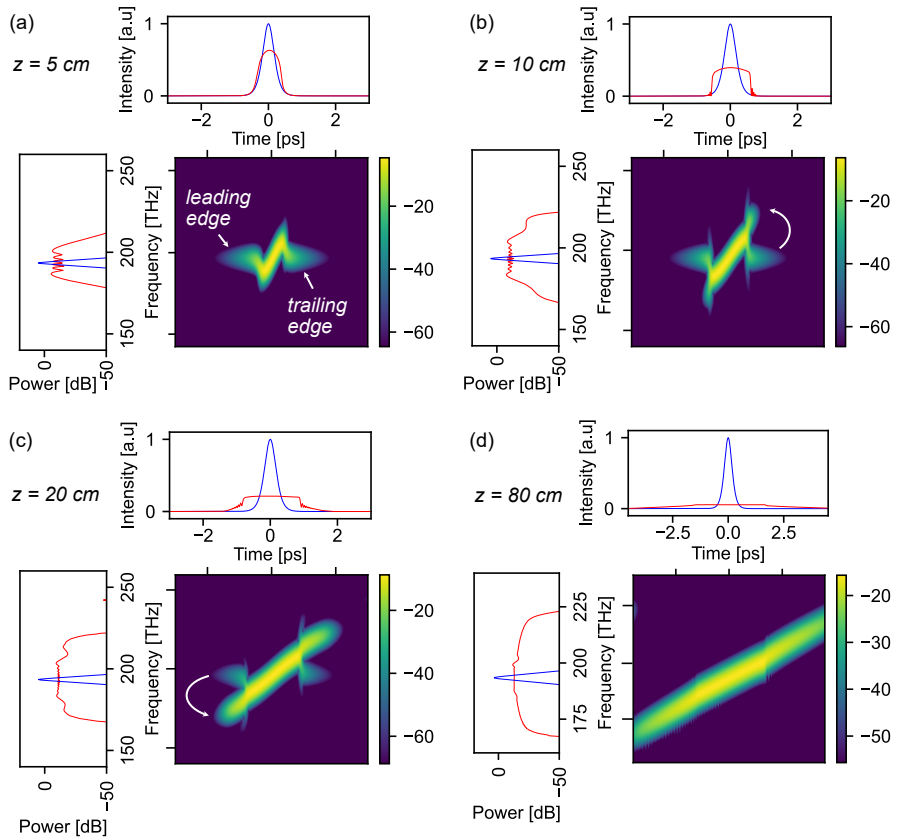

Figure 3.2: Spectrograms simulated using a Gaussian pulse with duration of 400 fs and 280 pJ in an all-normal dispersion waveguide with a dispersion β_2 of $+40$ ps^2·km^{-}1 at different propagations lengths, (a) 5 cm, (b) 10 cm, (c) 20 cm and (d) 80 cm.

self-phase modulation.

The reason for the nonlinear dynamics in this case, where SPM is being dominant over the dispersion, is because the nonlinear length $L_{NL} = (\gamma P_0)^{-1}$ is shorter than the propagation $L_D = T_0^{-1}/|\beta_2|$. Here T_0 and P_0 are the duration and peak power of the initial pulse. After a longer propagation, the dispersion takes over the nonlinear dynamics. This occurs due to the fact that the group velocity increases monotonically since all wavelengths exhibit normal dispersion. As a result, the trailing and leading edges of the pulse are steepened and OWB occurs.

This temporal overlap of the pulse frequency components translates into the creation of new frequency components via four-wave mixing [130]. This can be already observed at a propagation length of 10 cm, where a characteristic shoulder of OWB starts to appear at one of the edges of the spectrum (Figure 3.2 (b)). As the pulse propagates further, OWB transfers energy from the central frequency region to the other edge (Figure 3.2 (c)), causing a flattening of the spectrum. These interactions show that the maximum achievable bandwidth mainly depends on the initial SPM-induced broadening, which is defined as [127]

$$|\omega_{SPM}(z,t) - \omega_0| = \gamma P_0 \frac{\partial U(t)}{\partial t} z, \tag{3.4}$$

where U(t) is the normalized intensity of the pulse and z is the propagation distance. It is useful to analyze the spectrograms to get a better insight into the broadening. The initial S-shape is formed due to the self-frequency shift where the leading edge of the pulse is shifted to lower frequencies and the trailing of the pulse to higher frequencies. The central part experiences a linear shift, commonly referred to as a chirp. As OWB occurs, the energy is transferred from the center to the edges (see white arrows in Figure 3.2 (b,c)) causing a linear chirp across the pulse. Figure 3.2 (d) shows the spectrogram after further propagation, given the energy re-distribution caused by OWB, where the frequencies do not overlap temporally anymore. Therefore, the spectrum looks flat because of the absence of spectral interference and the chirp is completely linear.

Due to the temporal overlapping of the spectral components of the pulse, OWB is highly sensitive to the input pulse characteristics. In paper A, the ANDi waveguide was pumped using a femtosecond MLL, where the coupling was performed in free space to avoid undesired pulse broadening in fiber prior to propagation. When pumping with an electro-optic comb, an iterative pulse shaping technique was employed in order to maintain a transform-limited input pulse. This ensures a high peak power in both pumping schemes, however, due to the nonlinearities of the built-in amplifiers of the system, it is challenging to completely overcome the complex structure of the pump pulses that is translated to the broadened spectrum.

3.2 Kerr frequency combs in microresonators

Another approach for implementing an integrated frequency comb is the microresonator-based Kerr comb [85]. In this case, the nonlinear optical component is not a straight waveguide but a high-quality factor (Q) microresonator. The Kerr-comb generation relies on the third-order nonlinearity of the material in order to observe optical parametric generation. This Kerr nonlinearity allows two photons from the pump with a frequency ω_p to generate two photons at signal and idler frequencies, named four-wave mixing (FWM). Kerr nonlinearity-induced optical parametric oscillation in microcavities was first reported in [131,132]. In these works a toroidal micro-cavity with a high-Q allowed comb generation with low pump power. However, it was not until 2007 that frequency combs with broad optical bandwidth were demonstrated [46]. In that work, the parametric oscillation was followed by cascaded four-wave mixing, resulting in a 500 nm optical bandwidth. That demonstration not only showed a wide spectral bandwidth of the generated comb but also a constant line spacing across the spectrum [133].

Besides the use of toroidal micro-cavities, the demonstration of optical parametric oscillators in integrated planar resonators was also reported [49]. The use of silicon nitride drew significant attention due to the fact that it does not suffer from two-photon absorption in the near-IR as is the case for silicon [134]. Furthermore, in [49] it was shown to be possible to fabricate thicker waveguides which enabled the waveguide dispersion to be engineered to enhance FWM processes. However, it is worth mentioning that these FWM-based microresonator combs suffer from significant frequency and amplitude noise. The later demonstration of temporal dissipative solitons in [135] resulted in the formation of well-defined mode-locked waveforms, named dissipative Kerr solitons (DKS).

Similarly to optical fiber solitons, DKS relies on the balance between dispersion and non-linearities but with the extra addition of gain and loss interplay in the process [136]. The immediate effect of dispersion in microresonators is the deviation of the frequency location of the resonances. This causes the free-spectral range of the ring to become frequency-dependent. If the GVD of the fundamental mode of the microresonator is designed to operate in the normal dispersion region, the blue frequency components travel slower than the red ones. This means that the spacing between the resonances decreases as the frequency increases. Therefore, it is convenient to express the dispersion of the microresonator in terms

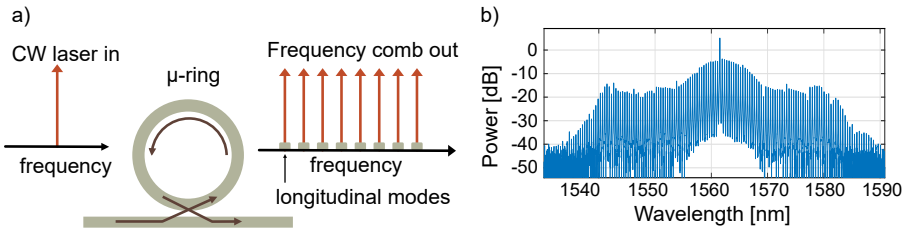

Figure 3.3: Concept of microcomb generation using a microring resonator. a) A single frequency C.W. laser is coupled to one resonance; the intracavity power builds up which allows the generation of new frequency components through nonlinear wave mixing. The repetition rate of the microcomb is governed by the free-spectral range of the cavity. b) Optical spectrum of a microcomb generated in the normal dispersion regime.

of the relative positions of the resonances, which can be described as an expansion around a central frequency according to [137, 138].

$$\omega_\mu = \omega_0 + D_1\mu + \frac{1}{2}D_2\mu^2 + \cdots, \tag{3.5}$$

Where ω_0 corresponds to the resonance used as the pump mode, the FSR of the resonator is related to $D_1/2\pi$. The parameter D_2 is linked to the GVD, and $D_2/2$ corresponds to the separation of the two FRS's nearest to the central frequency. The dispersion profile is then visualized using the integrated dispersion $D_{int} = \omega_\mu - (\omega_0 - D_1\mu)$.

The microcomb generation is sensitive to the sign of the microresonator dispersion, and it can turn into different waveform structures [84]. The first DKS microcomb was implemented in the anomalous dispersion regime where smooth hyperbolic secant-square spectral envelopes are obtained [139]. Another variant of DKS is the dark-soliton microcomb which is formed when the micro-resonator exhibits normal dispersion [140, 141]. In the next subsection, the mode-locked waveforms generated in the microresonator will be discussed.

3.2.1 Mode-locked Kerr microcombs

Mode-locking is attainable in microcombs by operating in the soliton regime, where a CW laser is converted into stable ultrashort pulses in the time domain [137, 139, 140, 142, 143]. Similarly to the SC generation, the group velocity dispersion inside the microresonator plays an important

role in the microcomb formation. The spectrum of microcombs generated in resonators with anomalous and normal dispersion are shown in Figure 3.4

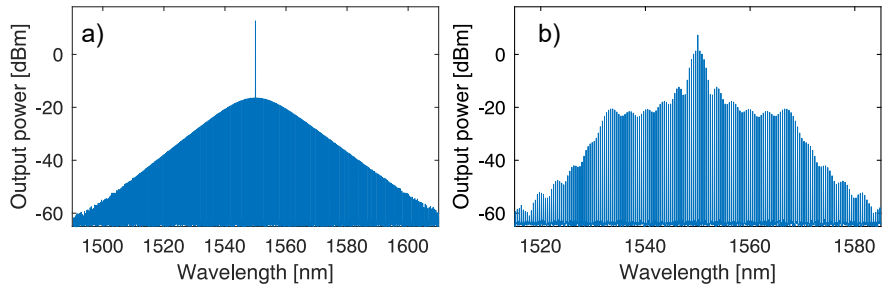

Figure 3.4: Kerr microcombs. a) A bright soliton featuring a hyperbolic spectral envelope is generated in a microresonator with anomalous dispersion. b) shows the spectrum of a dark pulse when the cavity dispersion is normal.

The processes occurring in nonlinear microcavities can be divided into two stages. The first one is modulation instability, also referred to as Turing rolls, where new equally spaced frequency components are generated. In the second stage, complex nonlinear dynamics including sub-comb formation and breathing states lead to comb formation [142]. For the initial growth of optical frequencies, it is necessary to access the modulation instability, which occurs when the CW field provides parametric amplification to other frequency components. When the gain compensates for the cavity losses, new frequency components are generated in the resonances of the cavity.

Mode-locking in the normal dispersion regime has been demonstrated theoretically and experimentally [140, 141, 144]. The comb generation in this regime is quite attractive for several reasons, for example, the dispersion of several bulk materials is normal in the visible and near IR spectral windows. Therefore, operating in the normal dispersion regime relaxes the dispersion engineering requirements. Other interesting aspects of the Kerr comb formation in the normal dispersion region are the deterministic behavior towards mode-locking and the high conversion efficiency [145–147].

A useful tool to model the dynamics of a microresonator with length L and intrinsic propagation losses α, is the Lugiato-Lefever equation [148]. This equation is also known as the externally driven, damped

nonlinear Schrödinger equation, due to the presence of an external driving field A_{in} with detuning.

$$T_R \frac{\partial A}{\partial t} = \left[\frac{\theta + \alpha L}{2} - i\delta_0 - iL\frac{\beta_2}{2}\frac{\partial^2}{\partial \tau^2} + iL\gamma|A|^2 \right] A + i\sqrt{\theta} A_{in}, \tag{3.6}$$

where T_R is the roundtrip time in the microresonator, A is the intracavity field, θ is the coupling coefficient between the bus waveguide and the ring, δ_0 is the detuning parameter of the cavity resonance from the pump frequency and A_{in} is the incident pump field.

The initiation of Kerr microcomb in normal DKS is experimentally challenging because of the difficulty of accessing the MI to grow the first comb lines. Although it is well known that MI existence requires anomalous dispersion in fibers, the MI in cavities may arise in both anomalous and normal dispersion [149]. In optical fibers, MI has been observed when a field interacts with another field with a different polarization or wavelength [127] and in fibers with periodic modulation of the GVD [150].

In optical microresonators, the mode interaction between the transverse and fundamental mode enables a localized anomalous dispersion which allows MI to occur [140, 141, 143]. These aided coupling interaction is however a product of accidental degeneracies in the spatial modes in the microresonator, making it difficult to control. This issue can be addressed by using a second cavity to induce the mode coupling, in this manner it is possible to control the coupling just by tuning the distance between the two rings. This was proposed in [146] where a dual-coupled ring arrangement induces mode coupling in a programmable way. Besides achieving mode-locking deterministically, the repetition rate of the comb can be tuned slightly by controlling the mode interaction location. A similar approach was performed in [147] where a microheater is placed on the auxiliary cavity to tune the avoided mode crossing location.

Mode-locked pulses generated in the normal dispersion regime, also called dark solitons, enable high power conversion efficiency [145–147]. Efficiency higher than 30 percent can be achieved due to the fact that the CW laser is detuned closer to the center of the resonance of the microresonator. For the generation of bright solitons in the anomalous dispersion regime, the pump CW laser is far red-detuned from the resonator resonance. Due to this large frequency detuning, a smaller portion of the CW laser power is coupled to the resonance and causes just a fraction to be converted into usable comb power. However, a recent work demonstrates that this limitation can be overcome by using a dual cavity architecture

to induce a frequency shift of the pump resonance, this in turn allows an unprecedented conversion efficiency [151].

In paper B, the experimental investigation of a microcomb in a dual-cavity configuration operating the normal dispersion is performed. The design of this dual-cavity design is similar to in [151], where the main cavity has a larger FSR than the auxiliary cavity. This enables a mode-crossing in a single resonance, which allows the formation of a dark-pulse structure, often called a platicon microcomb whose spectrum is symmetric and flat [141]. Two platicon microcombs were used to implement the first demonstration of dual-comb interferometry using microcombs operating in the normal dispersion regime.

Chapter 4

Dual-comb interferometry using microcombs

The optical frequency comb sources and their integration have been discussed in previous chapters. In this chapter, we will overview their application for dual-comb interferometry. First, the principle and the main generalities of the technique will be explained. The next subsections will cover the challenges and methods developed for performing dual-comb interferometry using microcombs in papers B and D.

4.1 Dual-comb interferometry

In paper C, different linear interferometric techniques using frequency combs were analyzed. Although these techniques can easily leverage the broad optical bandwidth of the comb, in order to exploit its frequency resolution, the individual comb lines should be fully resolved. This has been demonstrated employing dispersive and Fourier-transform (FT) interferometers [12, 152]. Implementations of Fourier transform spectrometers using frequency combs as the input source have notably increased the signal-to-noise ratio (SNR) due to their exceptional spatial coherence [12]. Despite the increased sensitivity, the initial deployment faced challenges in fully resolving the spectral lines, limited by the instrumental resolution dictated by the maximum path length of the interferometer. Nonetheless, recent demonstrations involving the coupling of frequency combs to FT spectrometers have successfully resolved the comb spectra by aligning the comb repetition rate with the spectrometer delay [153, 154]. The incorporation of enhancement cavities has further

increased the sensitivity by enabling a longer interaction path of the sample [155, 156].

An approach to Fourier transform interferometry uses an interferometer composed of two frequency combs, this technique is commonly referred to as dual-comb spectroscopy (DCS), which can deliver similar capabilities but avoids the use of movable components [157]. Instead, two combs with different repetition rates allow the mapping of the optical frequencies into the photo-detectable radio frequency domain. Using this technique, the second frequency comb is used to perform the spectral sampling and therefore dispense the need for a spectrometer [107, 158, 159]. DCS has been widely used to perform direct frequency comb spectroscopy using MLLs in the near-IR and in the mid-IR [11, 71, 160, 161].

DCS is unlikely to surpass FT spectroscopy in terms of spectral coverage, however, other features such as spectral resolution and accuracy are possible to attain using a comb-based approach. Furthermore, the development of DCS largely mirrors the growth of frequency comb generation. The advent of microcombs has opened up the possibility of using frequency combs for integrated spectrometers leveraging high SNR and fast acquisition rates. The outstanding phase noise characteristics in recent microcomb demonstrations make them even more appealing for DCS applications. However, the stabilization of microcombs is a key aspect to reach the fundamental resolution of DCS which is set by the linewidth of the comb tooth.

4.2 Operation principle

As mentioned earlier, DCS uses two frequency combs whose repetition rate has a slight frequency difference Δf_{rep} (see figure 4.1 (a,b)). The main idea is that these two combs interfere and generate a frequency comb in the RF domain composed of the pair-wise heterodyne beating of the frequency comb lines. In the RF domain, the sequence of beat notes is spaced by the difference of the repetition rate Δf_{rep}. In Figure 4.1 (b), the general idea of this concept is depicted. In the time domain, DCS can be understood as two trains of pulses with slightly different repetition rates, overlapping at the photodetector with varying delays. The photodetected signal results in the electric field cross-correlation which is sampled at time intervals $\Delta T = 1/f_{\mathrm{rep}}$, as shown in figure 4.1 (c).

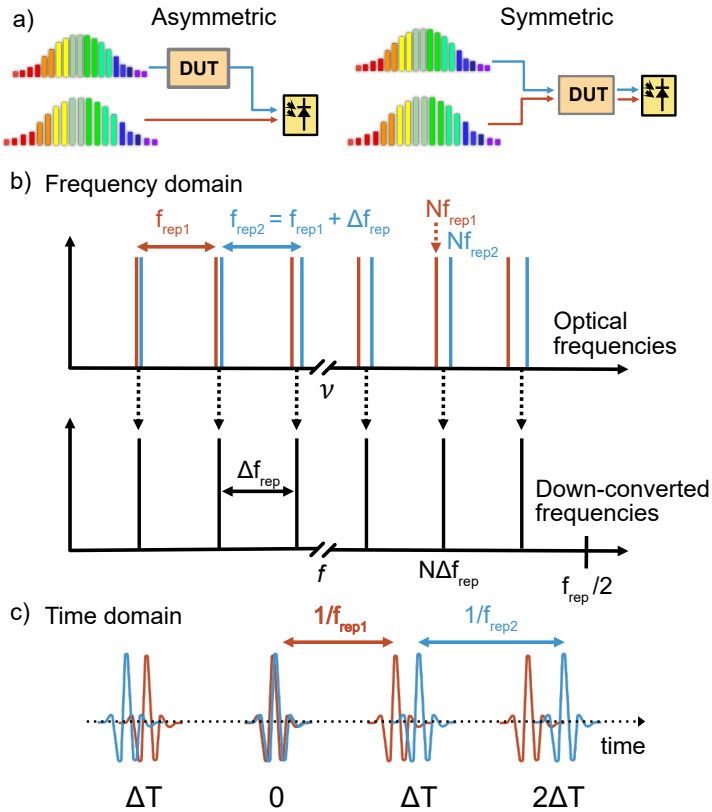

Figure 4.1: a) Dual-comb spectroscopy concept. A dual-comb interferometer can be implemented in an asymmetric (symmetric) configuration where the amplitude (and phase) of a device under test is encoded. b) Two frequency combs (red and blue) are mixed to produce a down-converted RF comb. c) In the time domain, a pulse-to-pulse walk-off between the two comb pulse trains is produced, i.e. a virtual scanning of a reference pulse over a signal pulse. The samples are recorded by a balanced photo-detector (BPD) at time intervals of ΔT using a real-time scope (RTS).

In order to perform spectroscopy, a sample under test is placed in one of the arms of the dual-comb interferometer. In this way, the response of the sample is encoded in the so-called signal comb and then sampled by the second comb, which is referred to as the local oscillator. This scheme allows for retrieval of both the amplitude and phase of the sample and is often called asymmetric or dispersive architecture [158]. Using

a symmetric approach is also possible, where the two combs interact with the sample, but only the amplitude of the comb, i.e. absorption features, are measured. In the following, the asymmetric approach will be considered.

Dual-comb spectroscopy is sometimes described in terms of electric-field cross-correlation (EFXC). In [109], this scheme was proposed for the characterization of optical arbitrary waveforms. It is possible to draw an analogy with traditional EFXC, where the cross-correlation between a signal pulse (a_s) and a reference pulse (a_r) is measured with respect to the delay (τ) of an interferometer. This delay is controlled by the mechanical translation of one of the arms of the interferometer. The interference is then recorded by a photo-detector yielding a time-averaged output power as in [162].

$$\langle P_{out}(t)\rangle = \frac{1}{2}\{U_r + U_s + [e^{j\omega_0\tau}\langle a_s(t)a_r^*(t-\tau)\rangle + c.c]\} \tag{4.1}$$

Where U_r and U_s are the energies of the pulses, these terms will correspond to DC components in the photo-detection. The oscillatory term measured as a function of the delay τ contains the information of the sample under test. Through Fourier analysis, it is then possible to retrieve the signal pulse if the reference pulse is known.

The same approach can be used in dual-comb interferometry, but instead, the delay is controlled by the difference in the repetition rate of the two combs. Therefore, the local oscillator pulse virtually scans the signal pulses, producing a cross-correlation interferogram with a period $1/\Delta f_{\text{rep}}$, as depicted in Figure 4.1(b). The Fourier transformation of the product of the electric field of both combs will simply translate to a radio-frequency comb. Since the difference in the repetition rate is the separation of the frequency lines of the RF domain, the bandwidth of the RF comb should not exceed half of the repetition rate. This is derived from the Nyquist condition and is maintained if the optical spectral bandwidth that is desired to acquire fulfills the following condition [158]:

$$\Delta\nu < \frac{m f_{\text{rep}}}{2} = \frac{f_{\text{rep}}^2}{2\Delta f_{\text{rep}}} \tag{4.2}$$

Where m is the so-called compression factor equal to $f_{\text{rep}}/\Delta f_{\text{rep}}$. If Δf_{rep} increases, the down-converted bandwidth will also increase, which will translate into aliasing. This means that by increasing the difference in repetition rate beyond this limit, the down-converted frequencies will

expand and overlap with the beating of higher-order frequencies. From equation 4.2, the maximum difference in repetition rate can be expressed as

$$\Delta f_{\mathrm{rep}} = \frac{f_{\mathrm{rep}}^2}{2\Delta\nu} \tag{4.3}$$

In terms of acquisition speed, the minimum time needed to acquire a single spectrum using DCS is given by $1/\Delta f_{\mathrm{rep}}$ at the expense of low SNR. One can realize that fast spectral acquisition is possible by increasing the difference in the repetition rate. Furthermore, as seen in equation 4.3, the acquisition speed scales with the repetition rate.

The SNR can be further increased by co-adding multiple successive spectra, i.e. coherent averaging. Therefore, improved SNR can be obtained without the need for long measurement acquisition times if an ultrafast single acquisition speed is performed. This scheme has been implemented using electro-optic combs [107–109, 163] and using microcombs in papers B and D.

4.3 Practical considerations using microcombs

Dual comb spectroscopy using microcombs involves several technical challenges, in this work, we have developed methods to realize this technique using platicon and bright soliton microcombs. In both cases, these microcombs are generated in photonic molecules, which have the advantage of diminishing the difficulties associated with comb formation. The deterministic microcomb generation, in addition to the spectral features of the microcomb such as high power per line and smooth spectra, is of significant interest for out-of-the-lab interferometry applications.

In order to consider every important parameter, it will be useful to first describe the experimental setup needed to generate the frequency combs and their down-mixing to the radio-frequency domain. Chapter five will explain in more detail the techniques used to characterize the microcombs generated and their stabilization.

4.3.1 Mutual coherence and repetition rate stability

Although the dynamics of microcomb generation are explained in the appended papers, some details on dual-comb interferometry are not explicit but yet important from an experimental point of view. For example, even though enforcing mutual coherence is not needed with the configuration

proposed here, dual-comb interferometry using microcombs can suffer from the drifting of the cavity detuning (δ_{comb}). This detuning is the difference in frequency between the pump laser and the pump resonance location, both being susceptible to drift over short-time scales.

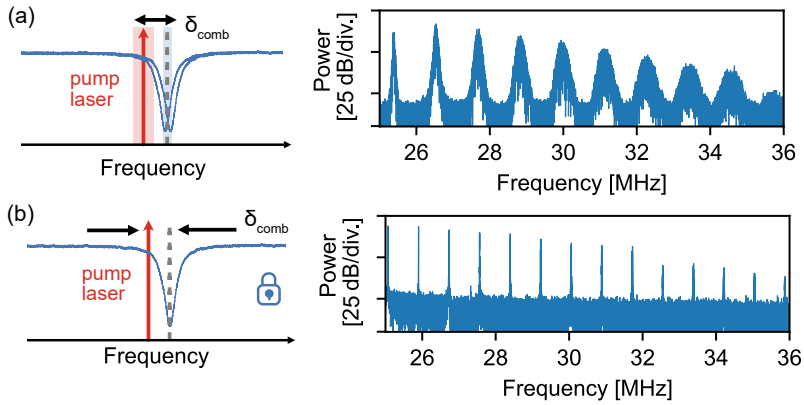

Figure 4.2: Dual-comb interferometry using microcombs and its dependence on the detuning. If the detuning of the microcomb is not fixed as shown in (a), the microcomb will not hold a low-noise state and the multiheterodyne spectra will exhibit a broadening of the linewidth. (b) If the detuning δ is locked, either by acting on the pump laser or the resonance of the cavity, the beat notes are well-resolved individual peaks.

There are two things that should be considered, the phase noise of the microcomb and the drift in the repetition rate. The former arises due to the fact that the microcomb can transition to a non-phase-locked state leading to a broadening in the optical linewidth of the comb. The latter is associated with the dispersion of the microcavity, causing changes in the repetition rate linked to the frequency of the pump. Both effects transfer to the down-mixed conversion, where a linewidth broadening of the RF comb lines is observed. Indeed, this was immediately noticed in the initial attempts to perform dual-comb using the microcombs. Figure 4.2 (a), shows an example of the dual-comb beating of microcombs in a high-noise state, where the beat note has significantly broadened due to the variations in the detuning. Once the comb detuning is fixed (see Figure 4.2 (b)) the RF comb is conformed by well-defined peaks, whose SNR can be further improved by coherently summing consecutive spectra.

After the combs have been generated and stabilized, one can proceed to the recording of dual-comb data. As shown in the simplified schematic

of the dual-comb interferometer 4.3 (a), (see Appendix A for the detailed list of components), the microcombs are generated by sharing the same pump laser and combined in a balanced photo-detector after one comb has interacted with the sample (4.3 (b)). By using a common pump, the generated combs will be phase-coherent by default. This, in turn, will cause the beatings of the microcomb's optical lines on the blue side of the pump to have the same frequency as the beatings on the red side. In Dutt et al [40], this was overcome using band-pass filters and extracting each side of the comb around the pump separately. Alternatively, in-phase/quadrature could avoid this limitation since the phase can be measured directly [80].

The strategy we followed to circumvent this ambiguity was to use an acousto-optic modulator (AOM) with a frequency of ~ 25 MHz inserted in one of the branches of the dual-comb interferometer. In this way, a unique RF frequency comes from beating each pair of the optical comb lines and it also moves the RF comb away from the baseband [107, 109]. Then the central frequency of the RF comb will be dictated by the AOM f_{AOM} and its frequency spacing by the difference in the repetition rate of the microcombs Δf_{rep} (4.3 (c)). In the time domain, these two frequencies will be reflected in the composition of the interferogram and its corresponding RF comb. We have studied two cases, being $\Delta f_{\mathrm{rep}} < f_{\mathrm{AOM}}$ and $\Delta f_{\mathrm{rep}} > f_{\mathrm{AOM}}$. To put this in context, the interferograms of dual-comb interferometry using a platicon microcomb and a bright soliton are depicted in Figure 4.3.

There is an intrinsic trade-off in the spectra acquisition between the detection bandwidth and the refresh rate since both are related to the repetition rate of the combs. The photo-detection bandwidth needed to map the downconverted comb can be calculated by multiplying the number of optical lines times Δf_{rep}.

Figure 4.3 (d) shows a zoom of an interferogram trace, where four complete interferograms are observed using platicon microcombs. Since the repetition rate of the platicon was controlled by means of its detuning, the difference in repetition rate of the platicons was in the kHz range ($\Delta f_{\mathrm{rep}} < f_{\mathrm{AOM}}$). The obtained RF comb will be localized in a 50 MHz region centered around f_{AOM}. In contrast, using two super-efficient solitons coming from different spatial locations of the same wafer, the repetition rate difference Δf_{rep} will result in higher than f_{AOM}. With these settings, the down-conversion will result in two interleaved RF combs as shown in Figure 4.3 (e). It is also clear that having a Δf_{rep}

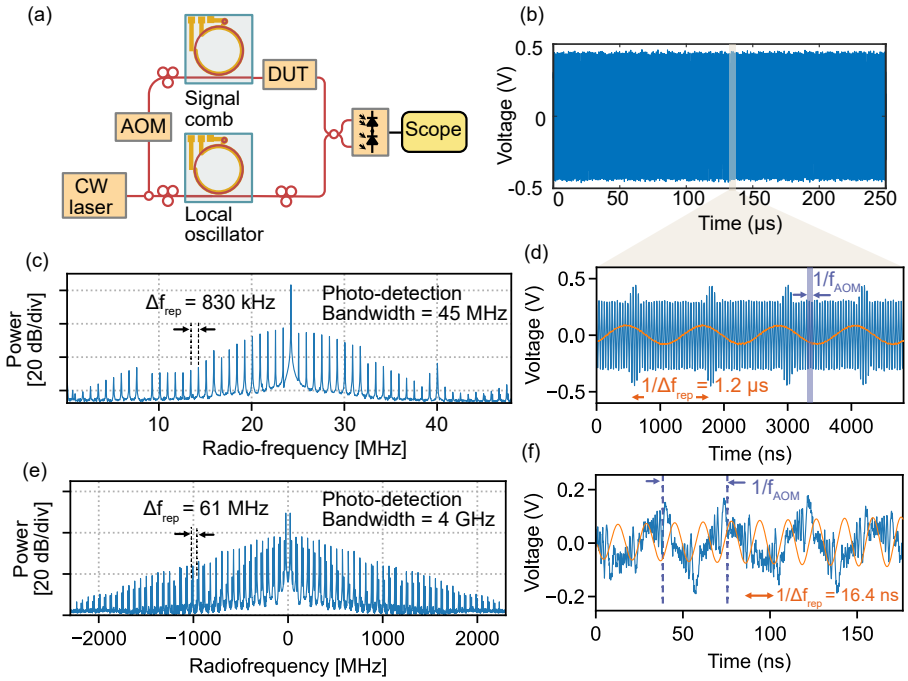

Figure 4.3: Dual-comb interferometry using microcombs. (a) A phase-sensitive configuration was used to perform dual-comb interferometry using platicon microcombs (b-d) and super-efficient microcombs (e, f), where one of the microcombs was used as a local oscillator and combined with a second microcomb that has interacted with a device under test. The photo-detected signal is recorded with a real-time sampling scope (b) the RF comb obtained assembles the spectral envelope of a platicon microcomb and is centered around f_{AOM} (c). (d) The interferogram is measured together with an RF signal that corresponds to the difference in the repetition rate Δf_{rep} of the combs (orange solid line). Using a super-efficient microcomb as shown in (e), the repetition rate Δf_{rep} is larger than f_{AOM}, resulting in two interlaced RF combs which are obtained from the Fourier transformation of the interferogram (f) constituted of a fringe pattern with period $(1/f_{\mathrm{AOM}})$ modulated by the cross-correlation of the combs (with a period of $1/f_{\mathrm{rep}}$).

in the order of tens of MHz will increase substantially the required sampling bandwidth, to the GHz range. On the other hand, the refreshing time between consecutive interferograms given by $1/f_{\mathrm{AOM}}$ is faster than the case where Δf_{rep} is in the order of kHz. These characteristics can enable the recording of the complete spectra in microseconds which can

be advantageous for applications where fast acquisition rates are needed.

4.3.2 Digital signal processing

The dual-comb interferometry experiments presented in papers B and D were performed using an asymmetric configuration, which yields both the magnitude and phase of the device under test. The low-noise state of the microcombs alleviates the digital processing since the down-converted comb lines are fully resolved. In this subsection, the process to extract the phase information of a device under test will be described, the code is available in [164].

Coherent averaging

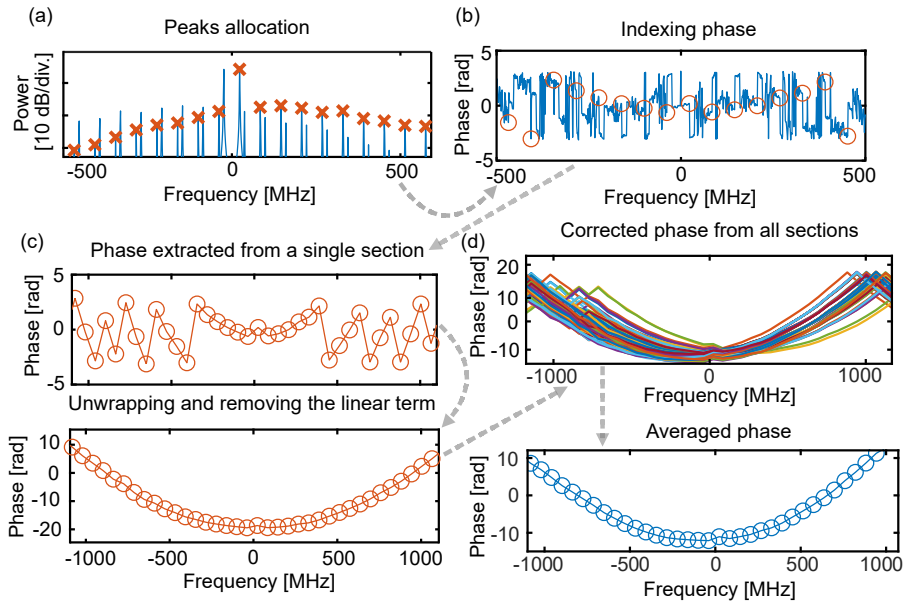

Figure 4.4: Post-processing of interferograms. (a) After the interferogram trace is cut into sections P composed of a number N of interferograms, they are Fourier-transformed to retrieve the phase and amplitude. Using a finding-peaks routine, the phase of the individual comb lines is retrieved. (c) The phase is then unwrapped and corrected removing the linear phase term. (d) A set of phase profiles with the same number of sections will be obtained and averaged to get the final phase response.

The data processing can be performed using different approaches and it is often that the recorded signal needs to be digitally corrected due to drifts in the repetition rate of the combs. The results presented in papers B and D account for this variation by extracting the difference in the repetition rate Δf_{rep} at the sampling stage. This information is extracted by measuring the repetition rate of each microcomb (f_{rep1} and f_{rep2}), which later passes through an RF circuit where both signals are mixed, filtered, and amplified. Further digital processing is made using a simple band-pass filter to obtain a pure sinusoidal signal. By extracting the zero crossings of this waveform it is possible to obtain the starting and ending point of each interferogram. The post-processed Δf_{rep} signal is shown together with the interferograms in Figure 4.3 (orange solid line).

Once the zero-crossing points have been obtained, they can be used to cut the recorded trace into individual interferograms. The recorded trace is divided into sections, where each contains the same number of interferograms N that will be processed. The number of interferograms per section is arbitrary but it should be large enough to resolve individual comb lines, in this way the signal-to-noise ratio is improved in comparison to using a single spectrum recorded in a time equal to $1/\Delta f_{\mathrm{rep}}$.

The individual sections are then Fourier transformed to extract the complex spectra. Using the amplitude information, a peak detection routine is employed to find the positions of the RF comb lines to be mapped, these peak locations are needed to index the phase information. Figure 4.4 shows the described process performed for each section. The extracted phase is then unwrapped and corrected by subtracting the linear phase term. After this step, a set of phase profiles is obtained and later averaged, which will yield the final result $\phi_{ref}(\omega)$.

Reference calibration measurement

To characterize a device under test with a phase $\phi_{\mathrm{DUT}}(\omega)$, it is needed to do a previous calibration of the dual-comb interferometer. For this purpose, two consecutive measurements are recorded, in one of them, the DUT is removed from the signal arm of the interferometer and will be considered the reference measurement. Both recorded datasets are post-processed using the same method described, therefore, two spectral phases are obtained, $\phi_{ref}(\omega)$ and $\phi_{meas}(\omega) = \phi_{ref}(\omega) \cdot \phi_{\mathrm{DUT}}(\omega)$. To obtain the response of the device under test, the complex transfer function of the interferometer can be removed by subtracting $\phi_{ref}(\omega)$ to $\phi_{meas}(\omega)$.

The device under test used for the experiments performed in papers B and D was a pulse shaper where instead of physically disconnecting the sample, two different filters can be programmed, one with a zero phase and a second simulating the DUT.

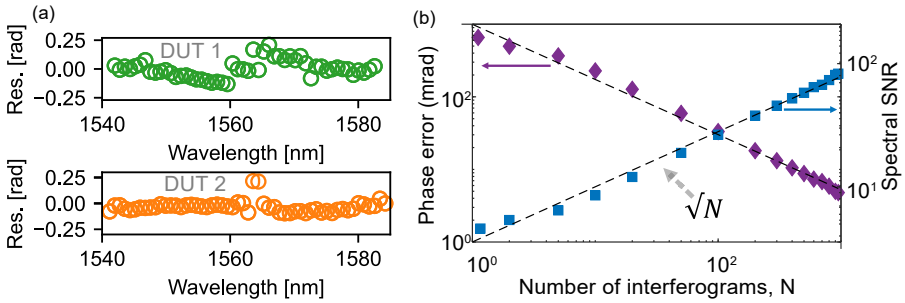

Figure 4.5: Phase error of dual-comb measurements. (a) Calculated residuals between the experimental phase recovered and the theoretical phase programmed in a pulse shaper. (b) Evolution of the signal-to-noise ratio and phase error using a number N of averaged interferograms.

Once the calibration of the interferometer is performed, the reference phase $\phi_{ref}(\omega)$ can be used for different samples (considering the optical components are maintained). Figure 4.4 (a) shows the residuals obtained by comparing the experimental results with the programmed curve in two different filters used as devices under test. The stand deviation of these residuals is 0.07 radians. Additionally, one can consider the frequency-domain signal-to-noise ratio (SNR_f) that can be calculated as the inverse of the phase error, $\sigma_\phi^{-1}(\nu)$ [108]. This metric is helpful to illustrate the potential of the coherent averaging process described above, as the phase error can be calculated for a different number of interferograms. Figure 4.5 (b) shows the evolution of SNR_f and the phase error calculated from 1000 interferograms coherently averaged. It is clear that by increasing the number of interferograms, the SNR_f scales close to $\sqrt{N}$ at the expense of increasing the refresh time given by $\Delta f_{\text{rep}} \cdot N$ and the phase error diminishes at the inverse of the SNR_f. Finally, it is worth mentioning that the outlined post-processing procedure can be executed using a field-programmable gate array (FPGA), which can utilize the coherent averaging process in real time. This approach circumvents the need for acquiring large datasets and enables the implementation of infinitely long averaging times [165].

Chapter 5

Microcombs characterization and control

This chapter will describe the techniques used for the stabilization and characterization of microcombs reported in the appended papers. These methods enabled the realization of dual-comb interferometry using microcombs in papers B and D, and long-term stabilization and sweeping keeping a coherent microcomb in papers E and F.

5.1 Microcomb stabilization

In the previous chapter, the importance of maintaining a coherent microcomb state since the linewidth of the comb teeth broadens as the microcomb transitions to a high-noise state was discussed. This is due to the fact that the properties of the microcomb will be determined by its pumping parameters such as the cavity-pump detuning δ_ω and the pump power. The cavity-pump detuning corresponds to the difference in frequency between the cavity δ_{cav} and the laser δ_{pump}.

$$\delta_\omega = \omega_{\text{cav}} - \omega_{\text{pump}}. \tag{5.1}$$

In the field of microcombs, it is said that the pump laser is blue-detuned if $\delta_\omega < 0$ and red-detuned when $\delta_\omega > 0$. Depending on the detuning regime, the soliton generated will exhibit different characteristics, hence its measurement and stabilization have been sought using different approaches [166–168]. The results presented in papers B, D-F relied on an indirect stabilization of the detuning using its dependency

with the soliton power (P_{sol}) [168, 169], as shown in the following equation:

$$P_{\mathrm{sol}} = \frac{2\eta A_{\mathbf{eff}}}{n_2 Q}\sqrt{-2n\beta_2\delta_\omega}, \tag{5.2}$$

where η is the coupling coefficient given by the ratio between the loaded quality factor of the cavity Q and the extrinsic quality factor Q_{ext}, β_2 is the group velocity dispersion, A_{eff} is the effective mode area, n and n_2 are the refractive index and nonlinear refractive index, respectively. An important remark by looking at this equation is that δ_ω and P_{sol} are the only parameters that can be tuned, as the others are fixed once the resonator is fabricated, thereby maintaining a one-to-one relation.

This approach is greatly simplified compared with other techniques that employ phase-sensitive locking such as using a network analyzer [167] or a Pound-Drever-Hall locking [170]. Nevertheless, since the photodetected comb power is used as a setpoint, the coupling power should be kept constant (using a fiber-packaged chip or an active-controlled coupling) to avoid power drifting.

As reported in paper E, the servo-control can be implemented by acting on the laser or the cavity. Choosing the former, the correction signal is fed back to the laser control, either on the piezo actuator or the current control. In the latter, the correction signal is fed back to the microheater placed on top of the resonator, keeping a fixed detuning by thermally tuning the resonance and forcing it to follow any drifts of the pump frequency. This thermal tuning is achieved due to thermo-optic (change of the refractive index n with temperature) and thermal expansion (change of the resonator length l with temperature) effects [171, 172], with a simple relation:

$$\frac{\partial f}{\partial T} = -f(\alpha_n + \alpha_l), \tag{5.3}$$

where α_n is the thermo-refractive coefficient and α_l is the thermal expansion coefficient. The thermal tuning is mainly attributed to the thermo-optic effect since α_l is one order of magnitude smaller than α_n in silicon nitride resonators, therefore the thermal expansion can be neglected when considering the tuning of the resonances [171, 173]. This effect was also exploited in paper F. where a microcomb was thermally tuned to fix the detuning and hence maintain a low-noise soliton state.

5.1.1 Detuning measurement

As mentioned earlier, δ_ω provides information on the distance in frequency between the pump laser and its corresponding resonance location, indicating whether it is blue- or red-detuned. In paper E, this measurement was conducted to assess the control of the locked system by probing the resonator with a counter-propagating laser [166]. The experimental arrangement is depicted in Figure 5.1 (a). While the frequency comb is generated, a "probe laser" is propagated in the backward direction with respect to the pump laser. This is achieved using two optical circulators. To measure the resonance, the probe laser is swept in frequency while maintaining low power to avoid non-linear effects. This light interferes with the back-scattered comb light due to imperfections in the microresonator, producing a beat note that varies over time depending on the frequency offset between the probe laser and the pump. It is worth noting that although the detuning was measured at the pump location, this measurement can be performed at any mode of the microresonator.

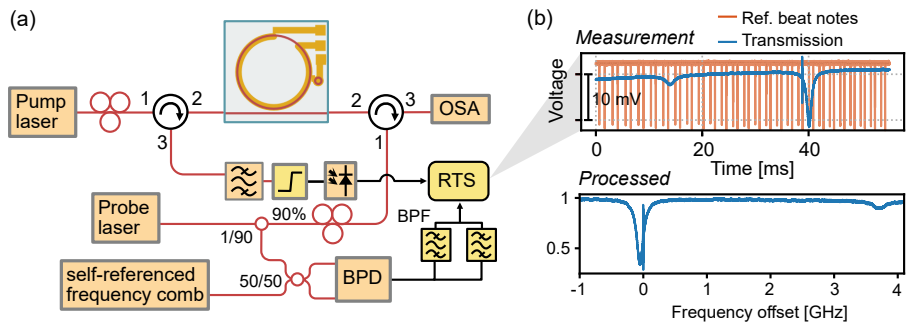

Figure 5.1: Setup for the measurement detuning in a microresonator. The detuning of the resonator is measured while generating a microcomb. (a) Schematic of the setup. A probe laser is injected into the microresonator in a counter-propagating manner using optical circulators. The beating produced with the pump laser is filtered optically and photo-detected. The electrical signal is then low-pass filtered and measured with a real-time scope (RTS). Reference beat notes are produced by heterodyning the probe laser with a self-referenced comb. (b) (Top) Measured transmission response and beat notes recorded as a function of time, (bottom) Normalized response with the calibrated frequency axis.

The measured detuning is shown in Figure 5.1 (b), where one can identify a dip in the transmission spectrum together with a sharp line cor-

responding to the beating between the probe laser and the back-reflected light. As the measurements are carried out in the time domain, calibration of the x-axis is necessary to determine the frequency detuning. This calibration can be accomplished with the assistance of a self-referenced frequency comb [174], which beat together with a portion of the probe laser (see Figure 5.1 (a)). The interference is detected using a balanced photo-detector, and the produced electrical signal passes through two band-pass filters at 30 and 75 MHz. In this way, beat markers are generated as the probe laser is scanned over time, which are recorded on the oscilloscope simultaneously with the resonance transmission spectrum. The post-processed data is shown in the bottom part of Figure 5.1.

5.2 Characterization techniques

As it was discussed earlier, a microcomb has two degrees of freedom, the pump frequency f_{pump} and the repetition rate frequency f_{rep}. Using the stabilization scheme described previously, we have minimized the excursions of these frequencies which can be employed in applications that depend on a stable and controlled microcomb output. The performance was then evaluated by measuring f_{rep} and f_{pump}, in the following these measurement techniques will be evaluated.

5.2.1 Repetition rate

The repetition rate of microcombs is usually THz for tens of GHz and it is given by the optical length of the microresonator. In planar technologies, there have been recent advancements in the fabrication methods to generate microcombs with a repetition rate compatible with current electronics bandwidth. Indeed, the platicon microcomb reported in paper B had a repetition rate of 50 GHz and can be directly photodetected. However, instruments with high-frequency bandwidth are required and can be employed up to a certain limit. Furthermore, if the aim is to generate a microcomb with a large spectral bandwidth, for example, covering a full octave, a high repetition rate (hundreds of GHz) is required and direct measurement is not possible [175]. This issue can be addressed using an electro-optic down-conversion technique [176].

In Figure 5.2 (a), the schematic of the setup employed is depicted. After the microcomb is generated, one portion of its optical power is sent to an electro-optic intensity modulator which is driven with a 25 GHz RF clock. The modulation produces side-bands to the comb lines

that will be proportional to the RF power sent to the modulator (see Chapter Two for details). If the number of side-bands (n) between the comb modes and the modulation frequency (f_{mod}) are properly chosen, the side-bands of two comb lines will meet in the center of the comb spacing and producing a beat note (f_{beat}). The repetition rate can be calculated as follows:

$$f_{\mathrm{rep}} = n \times f_{\mathrm{mod}} \pm f_{\mathrm{beat}} \tag{5.4}$$

The subtraction or addition of the beat note will depend if the side-bands have crossed each other or are nearby, respectively. This will be difficult to distinguish if f_{beat} has a lower frequency than the resolution of the optical spectrum analyzer (usually in the GHz range) and as shown in Figure 5.2 (b), the side-bands will appear to overlap. Therefore, to calculate f_{rep} prior information on the FSR of the microresonator will be needed. If the FSR is unknown, one can sweep the modulation frequency in a range of MHz and monitor the frequency of the beat note. If by increasing f_{mod}, the frequency of the beat note decreases, the side-bands have not crossed each other and f_{mod} should be added. On the contrary, the beat note should be substracted if its frequency increases at a higher f_{mod}.

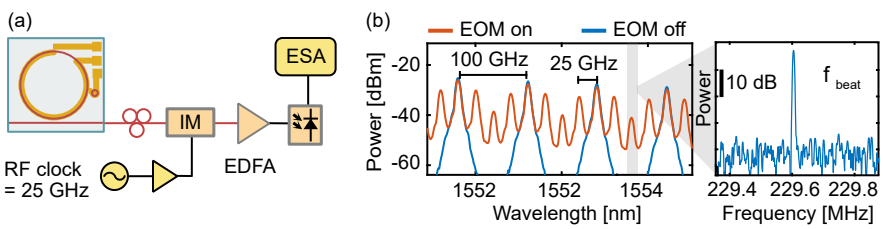

Figure 5.2: Electro-optic downconversion of the repetition rate. (a) The experimental setup consists of an electro-optic intensity modulator that is driven with a high-power RF signal that modulates a generated microcomb. An erbium-doped fiber amplifier is used to boost the optical signal and send it to a fast photo-detector. (b) Measured spectra using an optical spectrum analyzer of a microcomb with a repetition rate of 100 GHz (blue) and the output of the modulator (orange). The third-order sidebands of two neighboring comb lines produce a beat note in the MHz range.

5.2.2 Pump drifting monitoring

The implemented thermal locking maintains a fixed detuning, however, the frequency of the resonance and the pump laser can drift over a long time scale. To monitor the drifting of the pump frequency, the setup shown in Figure 5.3 was used. The optical layout is part of a commercial system of a self-referenced frequency comb, the light of the pump laser, and the frequency comb are collimated and combined using a beam splitter. A free-space grating is then used to spectrally filter a narrow band of the frequency comb together with the pump laser, which prevents the saturation of the photo-detector. This heterodyne process generates multiple beat notes between the pump laser and the frequency comb, which corresponds to the frequency offset of the pump with respect to the comb lines that are spaced at 250 MHz.

A single beat note is isolated using a low-pass filter and later amplified to be monitored using a spectrum analyzer as shown in the left of Figure 5.3. Although this process was realized only for monitoring the drifting of the pump frequency over time in paper E, the same signal could be used for a phase locking scheme. It would be needed to process the beat note using a digital phase comparator which outputs an error signal that can fed to a servo-control and generate a correction signal for the laser [177].

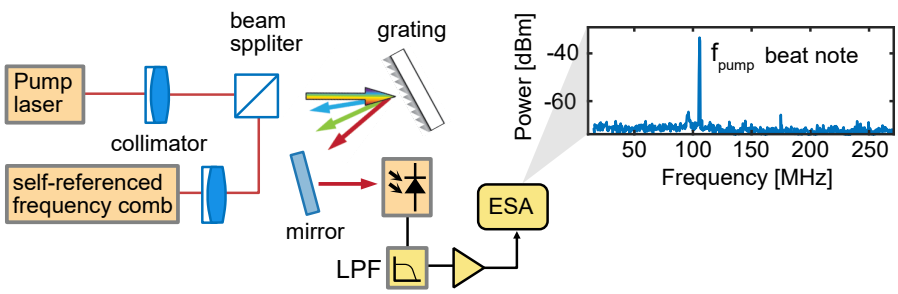

Figure 5.3: Setup of the measurement. The generation of a beat note between is made by spatially overlapping the collimated beams of the pump laser and a self-referenced comb. As the photo-detector will record the beating with multiple adjacent lines, the electrical signal is low-pass (LPF) filtered and later measured with an electrical spectrum analyzer (ESA).

Chapter 6

Future outlook

This thesis has focused on presenting techniques for conducting interferometry using chip-scale frequency combs. The research conducted explored the physics of on-chip frequency comb generation and addressed the various technical challenges associated with their implementation in dual-comb interferometry. In my opinion, there are a number of steps to be taken to fully harness the potential of microcombs out of the laboratory.

Integration of a turn-key dual-comb interferometer

From an engineering perspective and since many of the efforts on this thesis and ongoing research are to bring the photonic devices out of the lab, a natural step would be to package a ready-to-use dual-comb spectrometer. The experimental implementations were performed using state-of-the-art laboratory equipment, however, most of the instrumental can be replaced with single components once the operation of the microcomb has been characterized. For instance, the pump laser could be hybrid integrated into a silicon nitride chip [178–180], where two microcombs can be generated simultaneously [40]. This integration would eliminate the need for fiber connections by employing a single photonic integrated circuit. Furthermore, the large availability of electronics can also facilitate the development of an application-specific circuit, thereby automating comb generation and control, as well as the real-time acquisition and processing of data.

An instrument possessing the attributes of a dual-comb interferome-

ter could be adapted to explore other applications beyond spectroscopy. For instance, it could be tailored for ranging applications, allowing for the precise measurement of large distances. Additionally, it could find application in hyper-spectral imaging, enabling the spatial analysis of the spectral composition of specific samples. Such demonstrations have been reported in the literature, which highlights the versatility and potential of dual-comb interferometry beyond its use in spectroscopic analysis.

Combination of DCS with swept-wavelength interferometry

The spectral resolution attainable with DCS is fundamentally limited by the linewidth of the comb teeth. However, the spectral sampling is given by the repetition rate of the frequency comb. This spacing, which is typically in hundreds of GHz for microcombs, can be overcome with the combination of swept-wavelength interferometry [181, 182]. Using such an approach, the common pump laser is swept over the repetition rate span, which in turn reduces the resolution to narrower than the comb linewidth.

The challenge of implementing the sweeping of the pump laser lies in maintaining a constant detuning between the laser and the pump resonance [183]. This means that it is needed to tune the resonance of the main cavity over the full FSR of the comb while keeping a mode-locked state. This thesis work has laid out some of the foundations for the tuning of microcombs.

The key feature of realizing such a task is combining the high spectral resolution of swept-wavelength interferometry with a broad bandwidth frequency comb. Ideally, by using this technique it is possible to perform high-resolution spectroscopy over hundreds of nanometers. Applied to molecular spectroscopy, this would imply the massive characterization in parallel of multiple species.

Chapter 7

Summary of Papers

Paper A

Coherent supercontinuum generation in all-normal dispersion Si_3N_4 waveguides,
Optics Express, 30, 8641-8651, 2022.

In this paper we study the coherence properties of supercontinuum generation using straight waveguides in the normal dispersion regime. The spectrum of sub-picosecond pulses from an electro-optic comb with a high repetition rate is broadened by means of self-phase modulation in the normal dispersion. Pulses with higher energy with a femtosecond duration are also used as a pump source to access the optical wave-breaking regime.

My contributions: I assisted in the design of the waveguide and conducted the characterization of different samples. I conducted all the experiments for the generation and characterization of the supercontinuum. I wrote the paper with support from the co-authors and presented the work at CLEO Europe 2021.

Paper B

Platicon dynamics in photonic molecules,
Communication Physics, 6, 303, 2023.

In this work, we demonstrate the generation of a frequency comb in the normal dispersion regime using a dual-cavity architecture. An

important aspect of the design of this dual-cavity architecture is that the main cavity has a larger FSR than the auxiliary cavity. In this way, the avoided mode-crossing is only induced on a single resonance. As a consequence, the engineered comb spectra exhibit a symmetric and flat distribution characteristic of a platicon microcomb.

My contributions: I conducted all the lab experiments and made simulations for the study of the coupling between the repetition rate and pump detuning. I wrote the paper with support from the co-authors and presented part of the work at CLEO USA 2022.

Paper C

Frequency-comb-based spectral interferometry for characterization of photonic devices,
Micromachines, 13, no 4, p. 614, 2022.

We present a state-of-the-art concerning the use of frequency combs for spectral interferometry. The benefits leveraged by frequency combs are discussed using different interferometry configurations.

My contributions: I wrote the sections that describe the techniques of time and spectral domain and a sub-section of the applications. I assisted in the preparation of the complete manuscript.

Paper D

Super-efficient microcombs at the wafer level,
Submitted, 2023.

In this paper, we analyzed the yield of frequency comb generation in photonic molecule chips fabricated in the same wafer. We report a high fabrication yield of microcombs with a power conversion efficiency higher than 50 percent. We demonstrate their utilization for tri-comb phase-sensitive interferometry experiments which demonstrate the opportunities enabled by microcombs in a scalable platform.

My contributions: I performed multiple dual-comb interferometry where a single local oscillator was used to map the optical spectrum of two additional microcombs interacting with separate devices under test. I wrote the part of the manuscript related to comb interferometry.

Paper E

Active feedback stabilization of super-efficient microcombs, *Submitted*, 2023.

We experimentally demonstrate control of a super-efficient microcomb generated in a photonic molecule using the soliton power. Our findings demonstrate that our architectural approach effectively couples the effective comb detuning with the soliton power. Employing this method, we achieve the stabilization of a highly efficient microcomb indefinitely, enabling its practical deployment for dual-comb spectroscopy applications.

My contributions: I designed and implemented the experiments to perform the active stabilization of the microcomb. I wrote the paper and presented part of the results at CLEO Europe 2023.

Paper F

Thermal-controlled scanning of a bright soliton, *Proceedings of Conference on Lasers and Electro-Optics Europe/ European Quantum Electronics Conference (CLEO/Europe-EQEC)*, Munich, Germany, paper ed62, 2023.

We report the tuning of the modes of a bright soliton comb by thermally tuning the resonances of a photonic molecule. We implement a thermal control feedback system to maintain a soliton state over 60 GHz.

My contributions: I conceived the idea to perform the scanning of the microcomb and implemented the experiments. I wrote the paper and presented the results at CLEO Europe 2023.

Chapter 8

Appendices

Appendix A - Experimental setup to perform dual-comb interferometry using microcombs

The experiments discussed in Chapter 4 were conducted using the optical setup illustrated in Figure 8.1. The component specifications are outlined in Table 8.1. The generation of the combs involved two coupling stages (see the top-left of the figure), each comprising micro-positioners with piezo controllers and lensed fibers for light coupling. The chip was clamped in a temperature-controlled holder regulated by a thermistor, thermo-electric cooler, and PID controller, which facilitated stable temperature conditions. To apply an electrical current to the heaters, probing tungsten tips are placed on the electrical pad of the chips, the tips are mounted on individual micropositioners (Everbeing EB-050). Three pads are connected, a contact for the main cavity heater, an auxiliary heater, and a common pad used for grounding. These probes are connected to the AWG with a 1 mV resolution, although the AWG is usually configured as a DC supply, an arbitrary waveform can be programmed (in paper F, a square root function was needed).

After the microcombs are generated, the comb converted power (Conv.1 /Conv.2) is splitted for monitoring and for control using a Red Pitaya (RP), and a proportional-integral control loop is implemented using a python-based open-source package (PyrpL). One of the combs is sent to a pulse shaper (Finisar Waveshaper) where arbitrary filters are programmed. The combs are combined using a 3 dB coupler and sent to a balanced photo-detector which is later amplified. The output of the amplifier is connected directly to the oscilloscope to avoid electric delay

lines. The measurement of the repetition rate was done as specified in Figure 5.2. The components used for the RF circuit used for recording Δ_{rep} might differ from case to case since different power levels and spurious signals might require a different amplification or filtering. As a general advice, is important to monitor the RF power and the quality of the signal after each component. The specified components in table 8.1 were used for the dual-comb interferometry experiment using super efficient combs.

Component label	**Model**
CW laser	Toptica CTL
EDFA	Amonics AEDFA-33-B-FA
BPF1	Koshin Kogaku Filter
PC1, PC2	FPC032
AOM	Brimrose AMF-25-4-1550-2FP
PM 1-4	Power meters
AWG	Keysight 33522B
VA1, VA2	Voltage adder circuits
LPF	Thorlabs <52 MHz
RTS1	R&S RTA4004
FBG1, FBG2	AOS Tunable FBG
PD 1-4	Thorlabs DET08CFC
WS	Finisar Waveshaper
BPD	Thorlabs BDX3BA/BDX1EVB
RP1	Red Pitaya STEMlab 125-14
AMP1	JDS H301-1210
AMP2	Wenteq ABL0015-0012317
AMP3	Mini-circuits ZFL-1000LN+
AMP4	Picosecond 5840
MX	Mini-circuits ZFM-4
RTS2	Tektronix DSA71604

Table 8.1: List of components

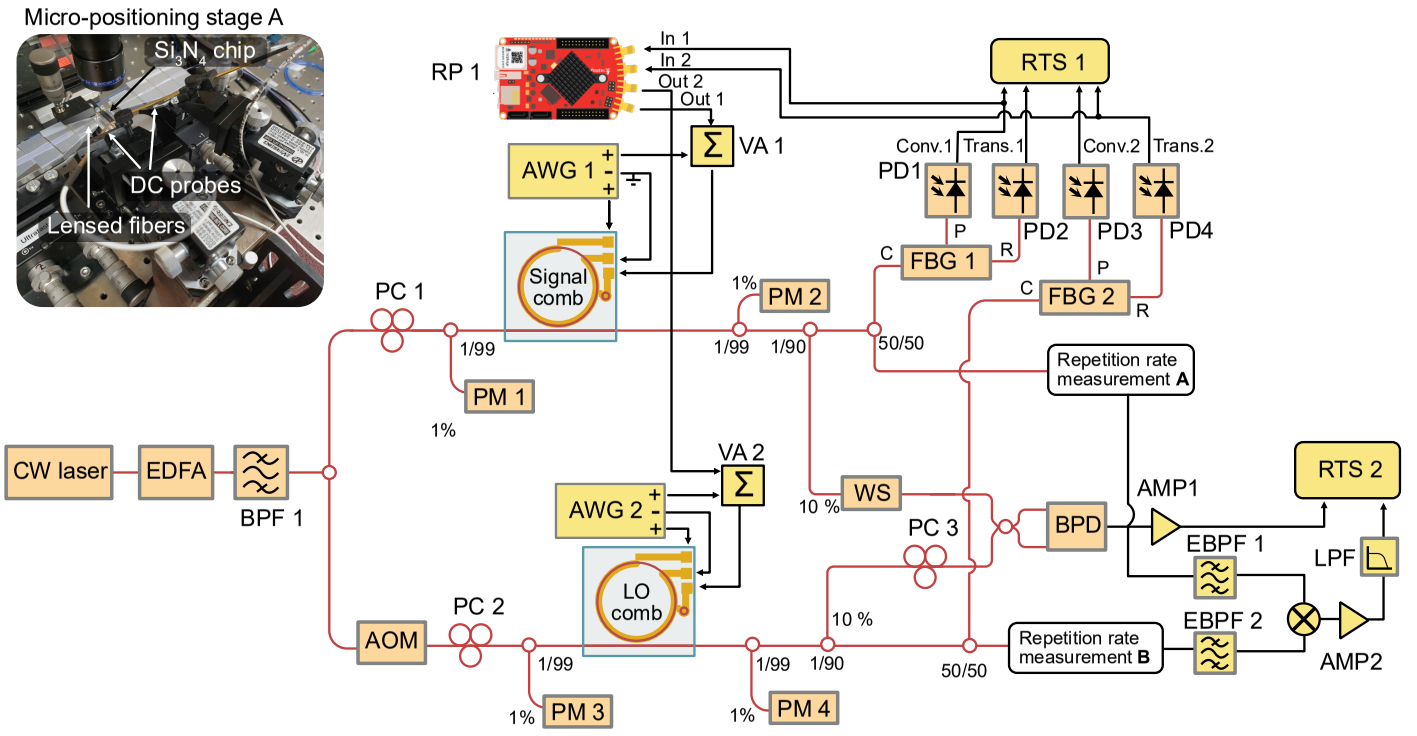

Figure 8.1: Setup. The diagram shows all the optical and electrical components used for the generation of microcombs, their stabilization, and utilization for dual-comb interferometry. EDFA: Erbium-doped fiber amplifier, AOM: Acousto-optic modulator, BPF: Band-pass filter, PC: Polarization controller, AWG: Arbitrary waveform generator, VA: Voltage adder, PM: Power meter, WS: Waveshaper, FBG: Fiber Bragg grating, PD: Photo-detector, BPD: Balanced photo-detector, AMP: Amplifier (electrical), EBPF: Electrical BPF, LPF: Low-pass filter, RTS: Real-time scope.

Appendix B - Free-space coupling of light into a nano-photonic waveguide

Here is a summary of the essential steps required to align free-space light into a waveguide, aimed to prevent the pulse distortion caused by nonlinear effects in fibers:

Free-space pumping

The pump pulse originates from a mode-locked laser within a commercial self-referenced comb system (Menlo FC1500). This femtosecond pulse is first amplified and then collimated to produce a free-space beam. As the beam has an initial diameter of approximately 2 mm, it necessitates expansion up to 8 mm to achieve a diffraction-limited spot of 2.4 micrometers, matching the mode field diameter of the waveguide.

The essential setup is depicted in Figure 8.2 (a). The collimated beam is directed to the beam expander (Thorlabs GBE05-C). Subsequently, the expanded beam passes through a $\lambda/2$ waveplate, serving to alter the polarization of the beam. Finally, the beam is directed towards an achromatic doublet (AC080-010-ML) featuring a focal length of 10 mm.

Alignment procedure

1. Place the achromatic doublet so that its center is roughly at the same level as the input of the waveguide in the "z" axis (propagation direction). Maintain an approximate distance between the edge of the lens and the input facet of the chip equal to the focal length.

2. Initially optimize the height of the micro-positioning stage supporting the chip. Monitor the light on the opposite side of the chip using a fluorescent card suitable for near-infrared light (ensure the environment light is dimmed for visibility). Adjust the height until an interference pattern is observed at the edge of the waveguide as shown in Figure 8.2 (b).

3. After observing the diffraction pattern, fine-tune the height until a clear beam profile is projected onto the detection card. Typically, this will be accompanied by the illumination of the waveguide, as illustrated in Figure 8.2 (c).

4. The last step is to adjust carefully the axis x, y and z of the micropositioner. To improve the coupling, I used a free-space power meter mounted in the chip holder, the area of the detector was covered

so that only light in the center was allowed to avoid scattered light from the input coupling. Finally, the polarization can be adjusted by rotating the $\lambda/2$ waveplate.

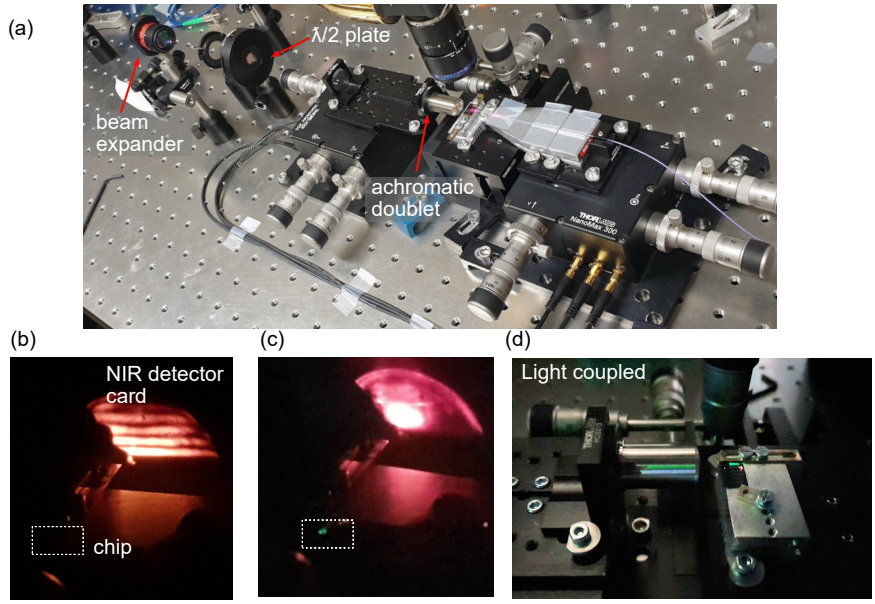

Figure 8.2: Free-space coupling. (a) Picture of the setup used to focus a collimated beam into a waveguide. To adjust the height, a near-infrared (NIR) detector card was used, and the height of the chip holder was first coarsely adjusted until a fringe pattern appeared (b). After reaching this point, the height is finely tuned until a beam profile is observed on the card. (c) Once the light is coupled, the waveguide is illuminated

References

[1] N. C. Thomas, "The early history of spectroscopy," *Journal of chemical education*, vol. 68, no. 8, p. 631, 1991.

[2] E. V. Loewenstein, "The history and current status of Fourier transform spectroscopy," *Applied Optics*, vol. 5, no. 5, pp. 845–854, 1966.

[3] P. R. Griffiths, "Fourier transform infrared spectrometry," *Science*, vol. 222, no. 4621, pp. 297–302, 1983.

[4] K.-N. Joo and S.-W. Kim, "Refractive index measurement by spectrally resolved interferometry using a femtosecond pulse laser," *Optics Letters*, vol. 32, no. 6, pp. 647–649, 2007.

[5] J. Park, J.-A. Kim, H. Ahn, J. Bae, and J. Jin, "A review of thickness measurements of thick transparent layers using optical interferometry," *International Journal of Precision Engineering and Manufacturing*, vol. 20, pp. 463–477, 2019.

[6] J. L. Hall, "Nobel Lecture: Defining and measuring optical frequencies," *Reviews of Modern Physics*, vol. 78, no. 4, pp. 1279–1295, 2006.

[7] T. W. Hänsch, "Nobel lecture: Passion for precision," *Reviews of Modern Physics*, vol. 78, no. 4, pp. 1297–1309, 2006.

[8] N. Picqué and T. W. Hänsch, "Frequency comb spectroscopy," *Nature Photonics*, vol. 13, no. 3, pp. 146–157, 2019.

[9] M. N. Fiddler, I. Begashaw, M. A. Mickens, M. S. Collingwood, Z. Assefa, and S. Bililign, "Laser spectroscopy for atmospheric and environmental sensing," *Sensors*, vol. 9, no. 12, pp. 10 447–10 512, 2009.

[10] Q. Liang, Y.-C. Chan, P. B. Changala, D. J. Nesbitt, J. Ye, and J. Toscano, "Ultrasensitive multispecies spectroscopic breath analysis for real-time health monitoring and diagnostics," *Proceedings of the National Academy of Sciences*, vol. 118, no. 40, p. e2105063118, 2021.

[11] F. Adler, P. Masłowski, A. Foltynowicz, K. C. Cossel, T. C. Briles, I. Hartl, and J. Ye, "Mid-infrared Fourier transform spectroscopy with a broadband frequency comb," *Opt. Express*, vol. 18, no. 21, pp. 21 861–21 872, 2010.

[12] J. Mandon, G. Guelachvili, N. Picqué, F. Druon, and P. Georges, "Femtosecond laser Fourier transform absorption spectroscopy," *Optics Letters*, vol. 32, no. 12, pp. 1677–1679, 2007.

[13] R. A. McCracken, J. M. Charsley, and D. T. Reid, "A decade of astrocombs: recent advances in frequency combs for astronomy," *Optics express*, vol. 25, no. 13, pp. 15 058–15 078, 2017.

[14] D. M. Lesko, H. Timmers, S. Xing, A. Kowligy, A. J. Lind, and S. A. Diddams, "A six-octave optical frequency comb from a scalable few-cycle erbium fibre laser," *Nature Photonics*, vol. 15, no. 4, pp. 281–286, 2021.

[15] A. Schliesser, N. Picqué, and T. W. Hänsch, "Mid-infrared frequency combs," *Nature Photonics*, vol. 6, no. 7, pp. 440–449, 2012.

[16] J. J. McFerran, W. C. Swann, B. R. Washburn, and N. R. Newbury, "Elimination of pump-induced frequency jitter on fiber-laser frequency combs," *Optics Letters*, vol. 31, no. 13, pp. 1997–1999, 2006.

[17] R. Bell, *Introductory Fourier transform spectroscopy*. Elsevier, 2012.

[18] P. Edwards, C. Zhang, B. Zhang, X. Hong, V. K. Nagarajan, B. Yu, and Z. Liu, "Smartphone based optical spectrometer for diffusive reflectance spectroscopic measurement of hemoglobin," *Scientific Reports*, vol. 7, no. 1, pp. 1–7, 2017.

[19] E. Ryckeboer, R. Bockstaele, M. Vanslembrouck, and R. Baets, "Glucose sensing by waveguide-based absorption spectroscopy on a silicon chip," *Biomed. Opt. Express*, vol. 5, no. 5, pp. 1636–1648, 2014.

[20] A. J. Das, A. Wahi, I. Kothari, and R. Raskar, "Ultra-portable, wireless smartphone spectrometer for rapid, non-destructive testing of fruit ripeness," *Scientific Reports*, vol. 6, no. 1, pp. 1–8, 2016.

[21] Z. Yang, T. Albrow-Owen, W. Cai, and T. Hasan, "Miniaturization of optical spectrometers," *Science*, vol. 371, no. 6528, p. eabe0722, 2021.

[22] A. J. McGonigle, T. C. Wilkes, T. D. Pering, J. R. Willmott, J. M. Cook, F. M. Mims, and A. V. Parisi, "Smartphone spectrometers," *Sensors*, vol. 18, no. 1, p. 223, 2018.

[23] N. Alshamrani, A. Grieco, B. Hong, and Y. Fainman, "Miniaturized integrated spectrometer using a silicon ring-grating design," *Optics Express*, vol. 29, no. 10, pp. 15 279–15 287, 2021.

[24] O. Schmidt, P. Kiesel, and M. Bassler, "Performance of chip-size wavelength detectors," *Optics Express*, vol. 15, no. 15, pp. 9701–9706, 2007.

[25] M. C. Souza, A. Grieco, N. C. Frateschi, and Y. Fainman, "Fourier transform spectrometer on silicon with thermo-optic non-linearity and dispersion correction," *Nature Communications*, vol. 9, no. 1, pp. 1–8, 2018.

[26] A. Nitkowski, L. Chen, and M. Lipson, "Cavity-enhanced on-chip absorption spectroscopy using microring resonators," *Opt. Express*, vol. 16, no. 16, pp. 11 930–11 936, 2008.

[27] S. Nezhadbadeh, A. Neumann, P. Zarkesh-Ha, and S. Brueck, "Chirped-grating spectrometer-on-a-chip," *Optics Express*, vol. 28, no. 17, pp. 24 501–24 510, 2020.

[28] B. Gao, Z. Shi, and R. W. Boyd, "Design of flat-band superprism structures for on-chip spectroscopy," *Opt. Express*, vol. 23, no. 5, pp. 6491–6496, 2015.

[29] G. Micó, B. Gargallo, D. Pastor, and P. Muñoz, "Integrated optic sensing spectrometer: Concept and design," *Sensors*, vol. 19, no. 5, 2019.

[30] P. Cheben, J. H. Schmid, A. Delâge, A. Densmore, S. Janz, B. Lamontagne, J. Lapointe, E. Post, P. Waldron, and D.-X. Xu, "A high-resolution silicon-on-insulator arrayed waveguide grating microspectrometer with sub-micrometer aperture waveguides," *Opt. Express*, vol. 15, no. 5, pp. 2299–2306, 2007.

[31] B. Momeni, E. S. Hosseini, and A. Adibi, "Planar photonic crystal microspectrometers in silicon-nitride for the visible range," *Opt. Express*, vol. 17, no. 19, pp. 17 060–17 069, 2009.

[32] X. Nie, E. Ryckeboer, G. Roelkens, and R. Baets, "CMOS-compatible broadband co-propagative stationary Fourier transform spectrometer integrated on a silicon nitride photonics platform," *Optics Express*, vol. 25, no. 8, pp. A409–A418, 2017.

[33] D. M. Kita, B. Miranda, D. Favela, D. Bono, J. Michon, H. Lin, T. Gu, and J. Hu, "High-performance and scalable on-chip digital fourier transform spectroscopy," *Nature Communications*, vol. 9, no. 1, pp. 1–7, 2018.

[34] A. V. Velasco, P. Cheben, P. J. Bock, A. Delâge, J. H. Schmid, J. Lapointe, S. Janz, M. L. Calvo, D.-X. Xu, M. Florjańczyk *et al.*, "High-resolution fourier-transform spectrometer chip with microphotonic silicon spiral waveguides," *Optics Letters*, vol. 38, no. 5, pp. 706–708, 2013.

[35] M. Nedeljkovic, A. V. Velasco, A. Z. Khokhar, A. Delâge, P. Cheben, and G. Z. Mashanovich, "Mid-infrared silicon-on-insulator Fourier-transform spectrometer chip," *IEEE Photonics Technology Letters*, vol. 28, no. 4, pp. 528–531, 2015.

[36] L. Chang, S. Liu, and J. E. Bowers, "Integrated optical frequency comb technologies," *Nature Photonics*, vol. 16, no. 2, pp. 95–108, 2022.

[37] S. M. Link, D. Maas, D. Waldburger, and U. Keller, "Dual-comb spectroscopy of water vapor with a free-running semiconductor disk laser," *Science*, vol. 356, no. 6343, pp. 1164–1168, 2017.

[38] J. Nürnberg, C. G. Alfieri, Z. Chen, D. Waldburger, N. Picqué, and U. Keller, "An unstabilized femtosecond semiconductor laser for dual-comb spectroscopy of acetylene," *Optics Express*, vol. 27, no. 3, pp. 3190–3199, 2019.

[39] M. Rösch, M. Beck, M. J. Süess, D. Bachmann, K. Unterrainer, J. Faist, and G. Scalari, "Heterogeneous terahertz quantum cascade lasers exceeding 1.9 thz spectral bandwidth and featuring dual comb operation," *Nanophotonics*, vol. 7, no. 1, pp. 237–242, 2018.

[40] A. Dutt, C. Joshi, X. Ji, J. Cardenas, Y. Okawachi, K. Luke, A. L. Gaeta, and M. Lipson, "On-chip dual-comb source for spectroscopy," *Science Advances*, vol. 4, no. 3, p. e1701858, 2018.

[41] M.-G. Suh, Q.-F. Yang, K. Y. Yang, X. Yi, and K. J. Vahala, "Microresonator soliton dual-comb spectroscopy," *Science*, vol. 354, no. 6312, pp. 600–603, 2016.

[42] M. Yu, Y. Okawachi, A. G. Griffith, N. Picqué, M. Lipson, and A. L. Gaeta, "Silicon-chip-based mid-infrared dual-comb spectroscopy," *Nature Communications*, vol. 9, no. 1, p. 1869, 2018.

[43] C. Bao, Z. Yuan, L. Wu, M.-G. Suh, H. Wang, Q. Lin, and K. J. Vahala, "Architecture for microcomb-based GHz-mid-infrared dual-comb spectroscopy," *Nature Communications*, vol. 12, no. 1, p. 6573, 2021.

[44] G. Villares, S. Riedi, J. Wolf, D. Kazakov, M. J. Süess, P. Jouy, M. Beck, and J. Faist, "Dispersion engineering of quantum cascade laser frequency combs," *Optica*, vol. 3, no. 3, pp. 252–258, 2016.

[45] D. Burghoff, Y. Yang, and Q. Hu, "Computational multiheterodyne spectroscopy," *Science advances*, vol. 2, no. 11, p. e1601227, 2016.

[46] P. Del'Haye, A. Schliesser, O. Arcizet, T. Wilken, R. Holzwarth, and T. J. Kippenberg, "Optical frequency comb generation from a monolithic microresonator," *Nature*, vol. 450, no. 7173, pp. 1214–1217, 2007.

[47] M. Zhang, B. Buscaino, C. Wang, A. Shams-Ansari, C. Reimer, R. Zhu, J. M. Kahn, and M. Lončar, "Broadband electro-optic frequency comb generation in a lithium niobate microring resonator," *Nature*, vol. 568, no. 7752, pp. 373–377, 2019.

[48] C. Wang, M. Zhang, M. Yu, R. Zhu, H. Hu, and M. Loncar, "Monolithic lithium niobate photonic circuits for Kerr frequency comb generation and modulation," *Nature Communications*, vol. 10, no. 1, p. 978, 2019.

[49] J. S. Levy, A. Gondarenko, M. A. Foster, A. C. Turner-Foster, A. L. Gaeta, and M. Lipson, "CMOS-compatible multiple-wavelength oscillator for on-chip optical interconnects," *Nature Photonics*, vol. 4, no. 1, pp. 37–40, 2010.

[50] J. Liu, G. Huang, R. N. Wang, J. He, A. S. Raja, T. Liu, N. J. Engelsen, and T. J. Kippenberg, "High-yield, wafer-scale fabrication of ultralow-loss, dispersion-engineered silicon nitride photonic circuits," *Nature communications*, vol. 12, no. 1, pp. 1–9, 2021.

[51] Z. Ye, K. Twayana, P. A. Andrekson *et al.*, "High-Q Si_3N_4 microresonators based on a subtractive processing for Kerr nonlinear optics," *Optics Express*, vol. 27, no. 24, pp. 35 719–35 727, 2019.

[52] J. Riemensberger, A. Lukashchuk, M. Karpov, W. Weng, E. Lucas, J. Liu, and T. J. Kippenberg, "Massively parallel coherent laser ranging using a soliton microcomb," *Nature*, vol. 581, no. 7807, pp. 164–170, 2020.

[53] P. Trocha, M. Karpov, D. Ganin, M. H. P. Pfeiffer, A. Kordts, S. Wolf, J. Krockenberger, P. Marin-Palomo, C. Weimann, S. Randel, W. Freude, T. J. Kippenberg, and C. Koos, "Ultrafast optical ranging using microresonator soliton frequency combs," *Science*, vol. 359, no. 6378, pp. 887–891, 2018.

[54] M.-G. Suh and K. J. Vahala, "Soliton microcomb range measurement," *Science*, vol. 359, no. 6378, pp. 884–887, 2018.

[55] H. Schnatz, B. Lipphardt, J. Helmcke, F. Riehle, and G. Zinner, "First phase-coherent frequency measurement of visible radiation," *Phys. Rev. Lett.*, vol. 76, pp. 18–21, 1996.

[56] S. A. Diddams, K. Vahala, and T. Udem, "Optical frequency combs: Coherently uniting the electromagnetic spectrum," *Science*, vol. 369, no. 6501, p. eaay3676, 2020.

[57] T. Fortier and E. Baumann, "20 years of developments in optical frequency comb technology and applications," *Communications Physics*, vol. 2, no. 1, p. 153, 2019.

[58] S. A. Diddams, "The evolving optical frequency comb [invited]," *Journal of the Optical Society of America B*, vol. 27, no. 11, p. B51, 2010.

[59] L. E. Hargrove, R. L. Fork, and M. A. Pollack, "Locking of he–ne laser modes induced by synchronous intracavity modulation," *Applied Physics Letters*, vol. 5, no. 1, pp. 4–5, 1964.

[60] H. W. Mocker and R. J. Collins, "Mode competition and self-locking effects in a q-switched ruby laser," *Applied Physics Letters*, vol. 7, no. 10, pp. 270–273, 1965.

[61] D. E. Spence, P. N. Kean, and W. Sibbett, "60-fsec pulse generation from a self-mode-locked Ti: sapphire laser," *Optics Letters*, vol. 16, no. 1, pp. 42–44, 1991.

[62] H. R. Telle, G. Steinmeyer, A. E. Dunlop, J. Stenger, D. H. Sutter, and U. Keller, "Carrier-envelope offset phase control: A novel concept for absolute optical frequency measurement and ultrashort pulse generation," *Applied Physics B*, vol. 69, no. 4, pp. 327–332, 1999.

[63] D. J. Jones, S. A. Diddams, J. K. Ranka, A. Stentz, R. S. Windeler, J. L. Hall, and S. T. Cundiff, "Carrier-envelope phase control of femtosecond mode-locked lasers and direct optical frequency synthesis," *Science*, vol. 288, no. 5466, pp. 635–639, 2000.

[64] J. Reichert, R. Holzwarth, T. Udem, and T. W. Hänsch, "Measuring the frequency of light with mode-locked lasers," *Optics Communications*, vol. 172, no. 1-6, pp. 59–68, 1999.

[65] J. K. Ranka, R. S. Windeler, and A. J. Stentz, "Visible continuum generation in air–silica microstructure optical fibers with anomalous dispersion at 800 nm," *Optics Letters.*, vol. 25, no. 1, pp. 25–27, 2000.

[66] S. A. Diddams, D. J. Jones, J. Ye, S. T. Cundiff, J. L. Hall, J. K. Ranka, R. S. Windeler, R. Holzwarth, T. Udem, and T. W. Hänsch, "Direct link between microwave and optical frequencies with a 300 THz femtosecond laser comb," *Physical Review Letters*, vol. 84, no. 22, pp. 5102–5105, 2000.

[67] T. Udem, R. Holzwarth, and T. W. Hänsch, "Optical frequency metrology," vol. 416, p. 5, 2002.

[68] V. Brasch, E. Lucas, J. D. Jost, M. Geiselmann, and T. J. Kippenberg, "Self-referenced photonic chip soliton Kerr frequency comb,"

Light: Science & Applications, vol. 6, no. 1, pp. e16 202–e16 202, 2017.

[69] F. Riehle, "Optical clock networks," *Nature Photonics*, vol. 11, no. 1, pp. 25–31, 2017.

[70] B. A. C. O. N. B. Collaboration, "Frequency ratio measurements at 18-digit accuracy using an optical clock network," *Nature*, vol. 591, no. 7851, pp. 564–569, 2021.

[71] F. Keilmann, C. Gohle, and R. Holzwarth, "Time-domain mid-infrared frequency-comb spectrometer," *Optics Letters.*, vol. 29, no. 13, pp. 1542–1544, 2004.

[72] V. Torres-Company and A. M. Weiner, "Optical frequency comb technology for ultra-broadband radio-frequency photonics," *Laser & Photonics Reviews*, vol. 8, no. 3, pp. 368–393, 2014.

[73] R. Zhuang, K. Ni, G. Wu, T. Hao, L. Lu, Y. Li, and Q. Zhou, "Electro-optic frequency combs: Theory, characteristics, and applications," *Laser & Photonics Reviews*, p. 2200353, 2023.

[74] A. J. Metcalf, V. Torres-Company, D. E. Leaird, and A. M. Weiner, "High-power broadly tunable electrooptic frequency comb generator," *IEEE Journal of Selected Topics in Quantum Electronics*, vol. 19, no. 6, pp. 231–236, 2013.

[75] V. Torres-Company, J. Lancis, and P. Andrés, "Lossless equalization of frequency combs," *Optics Letters.*, vol. 33, no. 16, pp. 1822–1824, 2008.

[76] S. Xiao, L. Hollberg, N. R. Newbury, and S. A. Diddams, "Toward a low-jitter 10 ghz pulsed source with an optical frequency comb generator," *Opt. Express*, vol. 16, no. 12, pp. 8498–8508, 2008.

[77] Y. Ozeki, S. Takasaka, M. Sakano, and S. Namiki, "Repetition rate variable and wavelength-tunable picosecond optical pulse source employing square-wave-driven intensity modulator and comb-like profiled fiber," *IEEE Photonics Technology Letters*, vol. 17, no. 12, pp. 2736–2738, 2005.

[78] I. Morohashi, T. Sakamoto, H. Sotobayashi, T. Kawanishi, and I. Hosako, "Broadband wavelength-tunable ultrashort pulse

source using a mach–zehnder modulator and dispersion-flattened dispersion-decreasing fiber," *Optics letters*, vol. 34, no. 15, pp. 2297–2299, 2009.

[79] D. R. Carlson, D. D. Hickstein, W. Zhang, A. J. Metcalf, F. Quinlan, S. A. Diddams, and S. B. Papp, "Ultrafast electro-optic light with subcycle control," *Science*, vol. 361, no. 6409, pp. 1358–1363, 2018.

[80] L. Lundberg, M. Mazur, A. Fiilöp, V. Torres-Company, and M. Karlsson, "Phase correlation between lines of electro-optical frequency combs," in *2018 Conference on Lasers and Electro-Optics (CLEO)*, 2018, pp. 1–2.

[81] K. Beha, D. C. Cole, P. Del'Haye, A. Coillet, S. A. Diddams, and S. B. Papp, "Electronic synthesis of light," *Optica*, vol. 4, no. 4, pp. 406–411, 2017.

[82] T. Ren, M. Zhang, C. Wang, L. Shao, C. Reimer, Y. Zhang, O. King, R. Esman, T. Cullen, and M. Lončar, "An integrated low-voltage broadband lithium niobate phase modulator," *IEEE Photonics Technology Letters*, vol. 31, no. 11, pp. 889–892, 2019.

[83] M. Yu, D. Barton III, R. Cheng, C. Reimer, P. Kharel, L. He, L. Shao, D. Zhu, Y. Hu, H. R. Grant *et al.*, "Integrated femtosecond pulse generator on thin-film lithium niobate," *Nature*, vol. 612, no. 7939, pp. 252–258, 2022.

[84] A. Pasquazi, M. Peccianti, L. Razzari, D. J. Moss, S. Coen, M. Erkintalo, Y. K. Chembo, T. Hansson, S. Wabnitz, P. Del'Haye, X. Xue, A. M. Weiner, and R. Morandotti, "Micro-combs: A novel generation of optical sources," *Physics Reports*, vol. 729, pp. 1–81, 2018.

[85] T. J. Kippenberg, R. Holzwarth, and S. A. Diddams, "Microresonator-based optical frequency combs," *Science*, vol. 332, no. 6029, pp. 555–559, 2011.

[86] C. Y. Wang, L. Kuznetsova, V. Gkortsas, L. Diehl, F. X. Kaertner, M. A. Belkin, A. Belyanin, X. Li, D. Ham, H. Schneider *et al.*, "Mode-locked pulses from mid-infrared quantum cascade lasers," *Optics Express*, vol. 17, no. 15, pp. 12 929–12 943, 2009.

[87] E. U. Rafailov, M. A. Cataluna, and W. Sibbett, "Mode-locked quantum-dot lasers," *Nature photonics*, vol. 1, no. 7, pp. 395–401, 2007.

[88] S. Ranta, A. Härkönen, T. Leinonen, L. Orsila, J. Lyytikäinen, G. Steinmeyer, and M. Guina, "Mode-locked vecsel emitting 5 ps pulses at 675 nm," *Optics letters*, vol. 38, no. 13, pp. 2289–2291, 2013.

[89] A. Jallageas, J. Nürnberg, C. G. Alfieri, D. Waldburger, S. M. Link, F. Emaury, J. Morel, and U. Keller, "Calibration of high-accuracy spectrometers using stabilized 11-ghz femtosecond semiconductor laser," *Optics Express*, vol. 27, no. 26, pp. 37 552–37 558, 2019.

[90] F. Lelarge, B. Dagens, J. Renaudier, R. Brenot, A. Accard, F. v. Dijk, D. Make, O. L. Gouezigou, J.-G. Provost, F. Poingt, J. Landreau, O. Drisse, E. Derouin, B. Rousseau, F. Pommereau, and G.-H. Duan, "Recent advances on inas/inp quantum dash based semiconductor lasers and optical amplifiers operating at 1.55 μm," *IEEE Journal of Selected Topics in Quantum Electronics*, vol. 13, no. 1, pp. 111–124, 2007.

[91] Y. Yang, D. Burghoff, J. Reno, and Q. Hu, "Achieving comb formation over the entire lasing range of quantum cascade lasers," *Optics Letters*, vol. 42, no. 19, pp. 3888–3891, 2017.

[92] D. Burghoff, T.-Y. Kao, N. Han, C. W. I. Chan, X. Cai, Y. Yang, D. J. Hayton, J.-R. Gao, J. L. Reno, and Q. Hu, "Terahertz laser frequency combs," *Nature Photonics*, vol. 8, no. 6, pp. 462–467, 2014.

[93] G. Scalari, J. Faist, and N. Picqué, "On-chip mid-infrared and THz frequency combs for spectroscopy," *Applied Physics Letters*, vol. 114, no. 15, p. 150401, 2019.

[94] M. Mazur, A. Lorences-Riesgo, J. Schröder, P. A. Andrekson, and M. Karlsson, "High spectral efficiency pm-128qam comb-based superchannel transmission enabled by a single shared optical pilot tone," *Journal of Lightwave Technology*, vol. 36, no. 6, pp. 1318–1325, 2018.

[95] T. Steinmetz, T. Wilken, C. Araujo-Hauck, R. Holzwarth, T. W. Hänsch, L. Pasquini, A. Manescau, S. D'Odorico, M. T. Murphy,

T. Kentischer, W. Schmidt, and T. Udem, "Laser frequency combs for astronomical observations," *Science*, vol. 321, no. 5894, pp. 1335–1337, 2008.

[96] M.-G. Suh, X. Yi, Y.-H. Lai, S. Leifer, I. S. Grudinin, G. Vasisht, E. C. Martin, M. P. Fitzgerald, G. Doppmann, J. Wang *et al.*, "Searching for exoplanets using a microresonator astrocomb," *Nature photonics*, vol. 13, no. 1, pp. 25–30, 2019.

[97] X. Yi, K. Vahala, J. Li, S. Diddams, G. Ycas, P. Plavchan, S. Leifer, J. Sandhu, G. Vasisht, P. Chen *et al.*, "Demonstration of a near-ir line-referenced electro-optical laser frequency comb for precision radial velocity measurements in astronomy," *Nature communications*, vol. 7, no. 1, p. 10436, 2016.

[98] M. Ludwig, F. Ayhan, T. M. Schmidt, T. Wildi, T. Voumard, R. Blum, Z. Ye, F. Lei, F. Wildi, F. Pepe *et al.*, "Ultraviolet astronomical spectrograph calibration with laser frequency combs from nanophotonic waveguides," *arXiv preprint arXiv:2306.13609*, 2023.

[99] V. Torres-Company, J. Schröder, A. Fülöp, M. Mazur, L. Lundberg, Ó. B. Helgason, M. Karlsson, and P. A. Andrekson, "Laser frequency combs for coherent optical communications," *Journal of Lightwave Technology*, vol. 37, no. 7, pp. 1663–1670, 2019.

[100] A. Jørgensen, D. Kong, M. Henriksen, F. Klejs, Z. Ye, Ò. Helgason, H. Hansen, H. Hu, M. Yankov, S. Forchhammer *et al.*, "Petabit-per-second data transmission using a chip-scale microcomb ring resonator source," *Nature Photonics*, vol. 16, no. 11, pp. 798–802, 2022.

[101] S. T. Cundiff and A. M. Weiner, "Optical arbitrary waveform generation," *Nature Photonics*, vol. 4, no. 11, pp. 760–766, 2010.

[102] N. B. Hébert, V. Michaud-Belleau, C. Perrella, G.-W. Truong, J. D. Anstie, T. M. Stace, J. Genest, and A. N. Luiten, "Real-time dynamic atomic spectroscopy using electro-optic frequency combs," *Physical Review Applied*, vol. 6, no. 4, p. 044012, 2016.

[103] N. Wilson, N. B. Hébert, C. Perrella, P. Light, J. Genest, S. Pustelny, and A. Luiten, "Simultaneous observation of nonlinear magneto-optical rotation in the temporal and spectral domains

with an electro-optic frequency comb," *Physical Review Applied*, vol. 10, no. 3, p. 034012, 2018.

[104] D. A. Long, A. J. Fleisher, D. F. Plusquellic, and J. T. Hodges, "Electromagnetically induced transparency in vacuum and buffer gas potassium cells probed via electro-optic frequency combs," *Optics Letters*, vol. 42, no. 21, pp. 4430–4433, 2017.

[105] D. R. Carlson, D. D. Hickstein, S. A. Diddams, and S. B. Papp, "High-speed ultra-broadband dual-comb spectroscopy using electro-optics," in *2018 Conference on Lasers and Electro-Optics (CLEO)*. IEEE, 2018, pp. 1–2.

[106] T. Nishikawa, A. Ishizawa, M. Yan, H. Gotoh, T. Hänsch, and N. Picqué, "Broadband dual-comb spectroscopy with cascaded-electro-optic-modulator-based frequency combs," in *CLEO: Science and Innovations*. Optical Society of America, 2015, pp. SW3G–2.

[107] P. Martin-Mateos, M. Ruiz-Llata, J. Posada-Roman, and P. Acedo, "Dual-comb architecture for fast spectroscopic measurements and spectral characterization," *IEEE Photonics Technology Letters*, vol. 27, no. 12, pp. 1309–1312, 2015.

[108] V. Durán, S. Tainta, and V. Torres-Company, "Ultrafast electrooptic dual-comb interferometry," *Opt. Express*, vol. 23, no. 23, pp. 30 557–30 569, 2015.

[109] F. Ferdous, D. E. Leaird, C.-B. Huang, and A. M. Weiner, "Dual-comb electric-field cross-correlation technique for optical arbitrary waveform characterization," *Optics Letters.*, vol. 34, no. 24, pp. 3875–3877, 2009.

[110] E. Deriushkina, I. R. Salgado, M. Mazur, V. Torres-Company, P. Andrekson, S. Gross, M. J. Withford, T. Hayashi, T. Nagashima, J. Schröder, and M. Karlsson, "Characterisation of a coupled-core fiber using dual-comb swept-wavelength interferometry," in *2021 European Conference on Optical Communication (ECOC)*, 2021, pp. 1–4.

[111] C. Joshi, A. Klenner, Y. Okawachi, M. Yu, K. Luke, X. Ji, M. Lipson, and A. L. Gaeta, "Counter-rotating cavity solitons in a silicon nitride microresonator," *Optics Letters*, vol. 43, no. 3, p. 547, 2018.

[112] C. Bao, M.-G. Suh, and K. Vahala, "Microresonator soliton dual-comb imaging," *Optica*, vol. 6, no. 9, pp. 1110–1116, 2019.

[113] M. Yu, Y. Okawachi, A. G. Griffith, M. Lipson, and A. L. Gaeta, "Microfluidic mid-infrared spectroscopy via microresonator-based dual-comb source," *Optics Letters.*, vol. 44, no. 17, pp. 4259–4262, 2019.

[114] Z. L. Newman, V. Maurice, T. Drake, J. R. Stone, T. C. Briles, D. T. Spencer, C. Fredrick, Q. Li, D. Westly, B. R. Ilic, B. Shen, M.-G. Suh, K. Y. Yang, C. Johnson, D. M. S. Johnson, L. Hollberg, K. J. Vahala, K. Srinivasan, S. A. Diddams, J. Kitching, S. B. Papp, and M. T. Hummon, "Architecture for the photonic integration of an optical atomic clock," *Optica*, vol. 6, no. 5, pp. 680–685, 2019.

[115] X. Ji, X. Yao, A. Klenner, Y. Gan, A. L. Gaeta, C. P. Hendon, and M. Lipson, "Chip-based frequency comb sources for optical coherence tomography," *Opt. Express*, vol. 27, no. 14, pp. 19 896–19 905, 2019.

[116] C. Bao, Z. Yuan, H. Wang, L. Wu, B. Shen, K. Sung, S. Leifer, Q. Lin, and K. Vahala, "Interleaved difference-frequency generation for microcomb spectral densification in the mid-infrared," *Optica*, vol. 7, no. 4, pp. 309–315, 2020.

[117] A. L. Gaeta, M. Lipson, and T. J. Kippenberg, "Photonic-chip-based frequency combs," *Nature Photonics*, vol. 13, no. 3, pp. 158–169, 2019.

[118] M. A. Foster, A. C. Turner, M. Lipson, and A. L. Gaeta, "Nonlinear optics in photonic nanowires," *Optics Express*, vol. 16, no. 2, pp. 1300–1320, 2008.

[119] R. Alfano and S. Shapiro, "Emission in the region 4000 to 7000 å via four-photon coupling in glass," *Physical Review Letters*, vol. 24, no. 11, p. 584, 1970.

[120] N. Singh, D. Vermulen, A. Ruocco, N. Li, E. Ippen, F. X. Kärtner, and M. R. Watts, "Supercontinuum generation in varying dispersion and birefringent silicon waveguide," *Optics Express*, vol. 27, no. 22, pp. 31 698–31 712, 2019.

[121] B. Kuyken, T. Ideguchi, S. Holzner, M. Yan, T. W. Hänsch, J. Van Campenhout, P. Verheyen, S. Coen, F. Leo, R. Baets, G. Roelkens, and N. Picqué, "An octave-spanning mid-infrared frequency comb generated in a silicon nanophotonic wire waveguide," *Nature Communications*, vol. 6, no. 1, pp. 1–6, 2015.

[122] R. Halir, Y. Okawachi, J. Levy, M. Foster, M. Lipson, and A. Gaeta, "Ultrabroadband supercontinuum generation in a CMOS-compatible platform," *Optics Letters*, vol. 37, no. 10, pp. 1685–1687, 2012.

[123] A. R. Johnson, A. S. Mayer, A. Klenner, K. Luke, E. S. Lamb, M. R. Lamont, C. Joshi, Y. Okawachi, F. W. Wise, M. Lipson *et al.*, "Octave-spanning coherent supercontinuum generation in a silicon nitride waveguide," *Optics Letters*, vol. 40, no. 21, pp. 5117–5120, 2015.

[124] H. Hu, F. Da Ros, M. Pu, F. Ye, K. Ingerslev, E. Porto da Silva, M. Nooruzzaman, Y. Amma, Y. Sasaki, T. Mizuno *et al.*, "Single-source chip-based frequency comb enabling extreme parallel data transmission," *Nature Photonics*, vol. 12, no. 8, pp. 469–473, 2018.

[125] H. Jung, C. Xiong, K. Y. Fong, X. Zhang, and H. X. Tang, "Optical frequency comb generation from aluminum nitride microring resonator," *Optics Letters*, vol. 38, no. 15, pp. 2810–2813, 2013.

[126] J. M. Dudley and J. R. Taylor, *Supercontinuum generation in optical fibers*. Cambridge University Press, 2010.

[127] G. P. Agrawal, *Nonlinear Fiber Optics*, 5th ed. Elsevier, 2012.

[128] J. M. Dudley and S. Coen, "Coherence properties of supercontinuum spectra generated in photonic crystal and tapered optical fibers," *Optics Letters.*, vol. 27, no. 13, pp. 1180–1182, 2002.

[129] C. Finot, B. Kibler, L. Provost, and S. Wabnitz, "Beneficial impact of wave-breaking for coherent continuum formation in normally dispersive nonlinear fibers," *J. Opt. Soc. Am. B*, vol. 25, no. 11, pp. 1938–1948, 2008.

[130] A. M. Heidt, J. S. Feehan, J. H. Price, and T. Feurer, "Limits of coherent supercontinuum generation in normal dispersion fibers," *JOSA B*, vol. 34, no. 4, pp. 764–775, 2017.

[131] T. J. Kippenberg, S. M. Spillane, and K. J. Vahala, "Kerr-nonlinearity optical parametric oscillation in an ultrahigh-Q toroid microcavity," *Phys. Rev. Lett.*, vol. 93, p. 083904, 2004.

[132] A. A. Savchenkov, A. B. Matsko, D. Strekalov, M. Mohageg, V. S. Ilchenko, and L. Maleki, "Low threshold optical oscillations in a whispering gallery mode CaF_2 resonator," *Phys. Rev. Lett.*, vol. 93, p. 243905, 2004.

[133] P. Del'Haye, O. Arcizet, A. Schliesser, R. Holzwarth, and T. J. Kippenberg, "Full stabilization of a microresonator-based optical frequency comb," *Phys. Rev.Lett.*, vol. 101, p. 053903, 2008.

[134] J. Leuthold, C. Koos, and W. Freude, "Nonlinear silicon photonics," *Nature Photonics*, vol. 4, no. 8, pp. 535–544, 2010.

[135] T. Herr, V. Brasch, J. D. Jost, C. Y. Wang, N. M. Kondratiev, M. L. Gorodetsky, and T. J. Kippenberg, "Temporal solitons in optical microresonators," *Nature Photonics*, vol. 8, no. 2, pp. 145–152, 2014.

[136] T. J. Kippenberg, A. L. Gaeta, M. Lipson, and M. L. Gorodetsky, "Dissipative Kerr solitons in optical microresonators," *Science*, vol. 361, no. 6402, p. eaan8083, 2018.

[137] T. Herr, V. Brasch, J. Jost, I. Mirgorodskiy, G. Lihachev, M. Gorodetsky, and T. Kippenberg, "Mode spectrum and temporal soliton formation in optical microresonators," *Physical Review Letters*, vol. 113, no. 12, p. 123901, 2014.

[138] P. Del'Haye, O. Arcizet, M. L. Gorodetsky, R. Holzwarth, and T. J. Kippenberg, "Frequency comb assisted diode laser spectroscopy for measurement of microcavity dispersion," *Nature Photonics*, vol. 3, no. 9, pp. 529–533, 2009.

[139] T. Herr, V. Brasch, J. D. Jost, C. Y. Wang, N. M. Kondratiev, M. L. Gorodetsky, and T. J. Kippenberg, "Temporal solitons in optical microresonators," *Nature Photonics*, vol. 8, no. 2, pp. 145–152, 2014.

[140] X. Xue, Y. Xuan, Y. Liu, P.-H. Wang, S. Chen, J. Wang, D. E. Leaird, M. Qi, and A. M. Weiner, "Mode-locked dark pulse Kerr combs in normal-dispersion microresonators," *Nature Photonics*, vol. 9, no. 9, pp. 594–600, 2015.

[141] V. Lobanov, G. Lihachev, T. Kippenberg, and M. Gorodetsky, "Frequency combs and platicons in optical microresonators with normal GVD," *Optics Express*, vol. 23, no. 6, pp. 7713–7721, 2015.

[142] T. Herr, K. Hartinger, J. Riemensberger, C. Wang, E. Gavartin, R. Holzwarth, M. Gorodetsky, and T. Kippenberg, "Universal formation dynamics and noise of Kerr-frequency combs in microresonators," *Nature Photonics*, vol. 6, no. 7, pp. 480–487, 2012.

[143] Y. Liu, Y. Xuan, X. Xue, P.-H. Wang, S. Chen, A. J. Metcalf, J. Wang, D. E. Leaird, M. Qi, and A. M. Weiner, "Investigation of mode coupling in normal-dispersion silicon nitride microresonators for kerr frequency comb generation," *Optica*, vol. 1, no. 3, pp. 137–144, 2014.

[144] P. Parra-Rivas, E. Knobloch, D. Gomila, and L. Gelens, "Dark solitons in the Lugiato-Lefever equation with normal dispersion," *Physical Review A*, vol. 93, no. 6, p. 063839, 2016.

[145] X. Xue, P. Wang, Y. Xuan, M. Qi, and A. M. Weiner, "Microresonator Kerr frequency combs with high conversion efficiency," *Laser & Photonics Reviews*, vol. 11, no. 1, p. 1600276, 2017.

[146] B. Y. Kim, Y. Okawachi, J. K. Jang, M. Yu, X. Ji, Y. Zhao, C. Joshi, M. Lipson, and A. L. Gaeta, "Turn-key, high-efficiency kerr comb source," *Optics Letters.*, vol. 44, no. 18, pp. 4475–4478, 2019.

[147] Ó. B. Helgason, F. R. Arteaga-Sierra, Z. Ye, K. Twayana, P. A. Andrekson, M. Karlsson, J. Schröder, and V. Torres-Company, "Dissipative solitons in photonic molecules," *Nature Photonics*, vol. 15, no. 4, pp. 305–310, 2021.

[148] L. A. Lugiato and R. Lefever, "Spatial dissipative structures in passive optical systems," *Physical Review Letters*, vol. 58, no. 21, p. 2209, 1987.

[149] S. Coen and M. Haelterman, "Modulational instability induced by cavity boundary conditions in a normally dispersive optical fiber," *Physical Review Letters*, vol. 79, no. 21, p. 4139, 1997.

[150] A. Mussot, M. Conforti, S. Trillo, F. Copie, and A. Kudlinski, "Modulation instability in dispersion oscillating fibers," *Advances in Optics and Photonics*, vol. 10, no. 1, pp. 1–42, 2018.

[151] Ó. B. Helgason, M. Girardi, Z. Ye, F. Lei, J. Schröder, and V. Torres-Company, "Surpassing the nonlinear conversion efficiency of soliton microcombs," *Nature Photonics*, pp. 1–8, 2023.

[152] S. A. Diddams, L. Hollberg, and V. Mbele, "Molecular fingerprinting with the resolved modes of a femtosecond laser frequency comb," *Nature*, vol. 445, no. 7128, pp. 627–630, 2007.

[153] P. Maslowski, K. F. Lee, A. C. Johansson, A. Khodabakhsh, G. Kowzan, L. Rutkowski, A. A. Mills, C. Mohr, J. Jiang, M. E. Fermann, and A. Foltynowicz, "Surpassing the path-limited resolution of Fourier-transform spectrometry with frequency combs," *Phys. Rev. A*, vol. 93, p. 021802, 2016.

[154] L. Rutkowski, P. Masłowski, A. C. Johansson, A. Khodabakhsh, and A. Foltynowicz, "Optical frequency comb fourier transform spectroscopy with sub-nominal resolution and precision beyond the Voigt profile," *Journal of Quantitative Spectroscopy and Radiative Transfer*, vol. 204, pp. 63–73, 2018.

[155] A. Głuszek, F. Senna Vieira, A. Hudzikowski, A. Wąż, J. Sotor, A. Foltynowicz, and G. Soboń, "Compact mode-locked er-doped fiber laser for broadband cavity-enhanced spectroscopy," *Applied Physics B*, vol. 126, no. 8, pp. 1–6, 2020.

[156] A. C. Johansson, L. Rutkowski, A. Khodabakhsh, and A. Foltynowicz, "Signal line shapes of fourier-transform cavity-enhanced frequency modulation spectroscopy with optical frequency combs," *J. Opt. Soc. Am. B*, vol. 34, no. 2, pp. 358–365, 2017.

[157] S. Schiller, "Spectrometry with frequency combs," *Optics Letters.*, vol. 27, no. 9, pp. 766–768, 2002.

[158] I. Coddington, N. Newbury, and W. Swann, "Dual-comb spectroscopy," *Optica*, vol. 3, no. 4, p. 414, 2016.

[159] Z. Chen, M. Yan, T. W. Hänsch, and N. Picqué, "A phase-stable dual-comb interferometer," *Nature Communications*, vol. 9, no. 1, pp. 1–7, 2018.

[160] Z. Chen, T. W. Hänsch, and N. Picqué, "Mid-infrared feed-forward dual-comb spectroscopy," *Proceedings of the National Academy of Sciences*, vol. 116, no. 9, pp. 3454–3459, 2019.

[161] C. Erny, K. Moutzouris, J. Biegert, D. Kühlke, F. Adler, A. Leitenstorfer, and U. Keller, "Mid-infrared difference-frequency generation of ultrashort pulses tunable between 3.2 and 4.8 μm from a compact fiber source," *Optics Letters.*, vol. 32, no. 9, pp. 1138–1140, 2007.

[162] A. Weiner, *Ultrafast optics*. John Wiley & Sons, 2011, vol. 72.

[163] G. Millot, S. Pitois, M. Yan, T. Hovhannisyan, A. Bendahmane, T. W. Hänsch, and N. Picqué, "Frequency-agile dual-comb spectroscopy," *Nature Photonics*, vol. 10, no. 1, pp. 27–30, 2016.

[164] I. Rebolledo-Salgado, "Dual-comb-interferometry-using-coherent-averaging: Post-processing code," zenodo: Version 1. 0. 4, October 2023, https://doi.org/10.5281/zenodo.10047374.

[165] I. Coddington, W. Swann, and N. Newbury, "Coherent dual-comb spectroscopy at high signal-to-noise ratio," *Physical Review A*, vol. 82, no. 4, p. 043817, 2010.

[166] P. Del'Haye, A. Coillet, W. Loh, K. Beha, S. B. Papp, and S. A. Diddams, "Phase steps and resonator detuning measurements in microresonator frequency combs," *Nature Communications*, vol. 6, no. 1, p. 5668, 2015.

[167] E. Lucas, H. Guo, J. D. Jost, M. Karpov, and T. J. Kippenberg, "Detuning-dependent properties and dispersion-induced instabilities of temporal dissipative kerr solitons in optical microresonators," *Phys. Rev. A*, vol. 95, p. 043822, 2017.

[168] X. Yi, Q.-F. Yang, K. Y. Yang, and K. Vahala, "Active capture and stabilization of temporal solitons in microresonators," *Optics Letters*, vol. 41, no. 9, pp. 2037–2040, 2016.

[169] X. Yi, Q.-F. Yang, K. Y. Yang, M.-G. Suh, and K. Vahala, "Soliton frequency comb at microwave rates in a high-Q silica microresonator," *Optica*, vol. 2, no. 12, pp. 1078–1085, 2015.

[170] Z. Ye, F. Lei, K. Twayana, M. Girardi, P. A. Andrekson, and V. Torres-Company, "Integrated, ultra-compact high-Q silicon nitride microresonators for low-repetition-rate soliton microcombs," *Laser & Photonics Reviews*, vol. 16, no. 3, p. 2100147, 2022.

[171] X. Xue, Y. Xuan, C. Wang, P.-H. Wang, Y. Liu, B. Niu, D. E. Leaird, M. Qi, and A. M. Weiner, "Thermal tuning of Kerr frequency combs in silicon nitride microring resonators," *Optics Express*, vol. 24, no. 1, pp. 687–698, 2016.

[172] A. Arbabi and L. L. Goddard, "Measurements of the refractive indices and thermo-optic coefficients of Si_3N_4 and SiO(x) using microring resonances," *Optics Letters*, vol. 38, no. 19, pp. 3878–3881, 2013.

[173] C. Joshi, J. K. Jang, K. Luke, X. Ji, S. A. Miller, A. Klenner, Y. Okawachi, M. Lipson, and A. L. Gaeta, "Thermally controlled comb generation and soliton modelocking in microresonators," *Optics Letters*, vol. 41, no. 11, pp. 2565–2568, 2016.

[174] K. Twayana, Z. Ye, Ó. B. Helgason, K. Vijayan, M. Karlsson *et al.*, "Frequency-comb-calibrated swept-wavelength interferometry," *Optics Express*, vol. 29, no. 15, pp. 24 363–24 372, 2021.

[175] P. Del'Haye, T. Herr, E. Gavartin, M. L. Gorodetsky, R. Holzwarth, and T. J. Kippenberg, "Octave spanning tunable frequency comb from a microresonator," *Phys. Rev. Lett.*, vol. 107, p. 063901, 2011.

[176] P. Del'Haye, S. B. Papp, and S. A. Diddams, "Hybrid electro-optically modulated microcombs," *Physical Review Letters*, vol. 109, no. 26, p. 263901, 2012.

[177] J. Jost, E. Lucas, T. Herr, C. Lecaplain, V. Brasch, M. Pfeiffer, and T. Kippenberg, "All-optical stabilization of a soliton frequency comb in a crystalline microresonator," *Optics Letters*, vol. 40, no. 20, pp. 4723–4726, 2015.

[178] A. S. Raja, A. S. Voloshin, H. Guo, S. E. Agafonova, J. Liu, A. S. Gorodnitskiy, M. Karpov, N. G. Pavlov, E. Lucas, R. R. Galiev *et al.*, "Electrically pumped photonic integrated soliton microcomb," *Nature communications*, vol. 10, no. 1, p. 680, 2019.

[179] B. Shen, L. Chang, J. Liu, H. Wang, Q.-F. Yang, C. Xiang, R. N. Wang, J. He, T. Liu, W. Xie *et al.*, "Integrated turnkey soliton microcombs," *Nature*, vol. 582, no. 7812, pp. 365–369, 2020.

[180] W. Jin, Q.-F. Yang, L. Chang, B. Shen, H. Wang, M. A. Leal, L. Wu, M. Gao, A. Feshali, M. Paniccia *et al.*, "Hertz-linewidth semiconductor lasers using cmos-ready ultra-high-q microresonators," *Nature Photonics*, vol. 15, no. 5, pp. 346–353, 2021.

[181] M. Mazur, N. K. Fontaine, M. Karlsson, P. A. Andrekson, J. Schröder *et al.*, "Dual-comb swept wavelength interferometry," in *CLEO: Applications and Technology*. Optica Publishing Group, 2020, pp. JW2B–23.

[182] E. Deriushkina, I. Rebolledo-Salgado, M. Mazur, V. Torres-Company, P. Andrekson, J. Schröder, and M. Karlsson, "Dual-comb swept-wavelength interferometry: Theory and experiment," *Journal of Lightwave Technology*, vol. 40, no. 19, pp. 6508–6516, 2022.

[183] T. Lin, A. Dutt, C. Joshi, X. Ji, C. T. Phare, Y. Okawachi, A. L. Gaeta, and M. Lipson, "Broadband ultrahigh-resolution chip-scale scanning soliton dual-comb spectroscopy," *arXiv preprint arXiv:2001.00869*, 2020.

Included papers A-F

Paper A

Israel Rebolledo-Salgado, Zhichao Ye, Simon Christensen, Fuchuan Lei, Krishna Twayana, Jochen Schröder, Martin Zelan, and Victor Torres-Company, "Coherent supercontinuum generation in all-normal dispersion Si_3N4 waveguides", *Optics Express*, 30, 8641-8651, 2022.

Paper B

Israel Rebolledo-Salgado, Óskar B. Helgason, Zhichao Ye, Jochen Schröder, Martin Zelan, and Victor Torres-Company, "Platicon dynamics in photonic molecules", *Communication Physics*, 6, 303, 2023.

Paper C

Krishna Twayana, **Israel Rebolledo-Salgado**, Ekaterina Deriushkina, Jochen Schröder, Magnus Karlsson and Victor Torres-Company, "Frequency-comb-based spectral interferometry for characterization of photonic devices", *Micromachines*, 13, no 4, p. 614, 2022.

Paper D

Marcello Girardi, Óskar B. Helgason, Carmen H. López Ortega, **Israel Rebolledo-Salgado** and Victor Torres-Company, "Super-efficient microcombs at the wafer level", *Submitted*, 2023.

Paper E

Israel Rebolledo-Salgado, Óskar B. Helgason, Vicente Durán, Marcello Girardi, Martin Zelan and Victor Torres-Company, "Active feedback stabilization of super-efficient microcombs in photonic molecules", *Submitted*.

Paper F

Israel Rebolledo-Salgado, Vicente Durán, Óskar B. Helgason, Marcello Girardi, Martin Zelan and Victor Torres-Company, "Thermal-Controlled Scanning of a Bright Soliton in a Photonic Molecule", *Proceedings of Conference on Lasers and Electro-Optics Europe/ European Quantum Electronics Conference (CLEO/Europe-EQEC)*, Munich, Germany, paper ed62, 2023.